journal of the international meteor organization

WGN

43:5
october 2015

Antihelion, apex and toroidal meteoroid sources explored
New high-declination showers discovered
Maribo meteorite linked to meteor shower and asteroid
May–June video meteors

ISSN 1016-3115

WGN Vol. 43, No. 5, October 2015, pp. 121 – 160

Conferences

Administrative

Meteor Science

Preliminary results

Front cover photo

Orionid fireball photographed on 2015 October 23 at $02^{\mathrm{h}}42^{\mathrm{m}}45^{\mathrm{s}}$ UT from Medvedje Brdo, Slovenia. It was shot using Canon 40D camera at ISO 800 equipped with 17 mm $f/2.8$ lens, and 59 s exposure. (See also development of the persistent train on the back cover.) Photo courtesy: Javor Kac.

Writing for WGN

This Journal welcomes papers submitted for publication. All papers are reviewed for scientific content, and edited for English and style. Instructions for authors can be found in WGN **31:4**, 124–128, and at `http://www.imo.net/docs/writingforwgn.pdf` .

Copyright

Legal address

International Meteor Organization, Jozef Mattheessensstraat 60, 2540 Hove, Belgium.

Conferences

Thirty-Fifth International Meteor Conference, Egmond, the Netherlands, June 2–5, 2016

Roy Keeris and Joost Hartman[1]

IMC 2016

June 2-5, Egmond - the Netherlands

Gorgeous dunes, vast views of the North Sea and rich smooth yellow cheese. Next year's International Meteor Conference (IMC 2016) will take place in the seaside town of Egmond, the Netherlands, from June 2 to 5, 2016. The program includes talks on the latest developments in meteor observing, poster sessions, and evening entertainment. In addition, we will embark on a big shrimp trawler and sail the shallow waters of the UNESCO and Dutch Heritage Site the Wadden Sea to catch fresh shrimp, which we will have for dinner. To participate, you must register no later than April 15, 2016, but booking before February 28, 2016, saves you 30 Euros. Moreover, registration may be closed early if full capacity is reached before the deadline, as was the case this year in Mistelbach. So, prospective participants have every reason not to delay their decision and to book early!

Organization

The International Meteor Conference is an annual event of the International Meteor Organization (IMO) held at a different location each year. The IMC 2016 will be hosted by the Meteor Section of the Royal Dutch Association for Meteorology and Astronomy (*Koninklijke Nederlandse Vereniging voor Weer- en Sterrenkunde* in Dutch, abbreviated "KNVWS"). The IMC 2016 takes place just before the Meteoroids 2016 Conference, held at ESTEC, Noordwijk, from June 6 to 10, a mere 50 km south of Egmond. This should stimulate participants of either conference to visit the other one as well, thus maximizing cross-fertilization between amateur and professional meteor astronomers. There is also a second reason why the IMC 2016 is a particularly festive event for the local organizers: in 2016, the KNVWS Meteor Section celebrates its 70th anniversary!

Figure 1 – Dutch coast and dunes.

[1]Email: imc2016@imo.net

Figure 2 – Left: Trawler fishing for shrimp on the Wadden Sea. *Right*: Seals resting on a sand strip.

Egmond, surroundings, and climate

The conference will be held at the Stayokay Hostel in Egmond. This hostel will be available exclusively for the conference and will serve as host for full-board participants. The Hostel is at walking distance from the Dutch beach, has three sun-dressed terraces, bikes, and numerous options, and is children-friendly. To participants who do not want to stay at the Stayokay Hostel, the LOC will provide assistace in arranging for alternative accommodation in the nearby village.

The Netherlands have a temperate climate. Early June has average temperatures of about 16° C in the afternoon and 10° C at night, but this may vary. While rain and showers are common, the Sun shines 7 hours a day on average in June.

Excursion: shrimp and seals

On Saturday afternoon, there will be an excursion to the Wadden Sea (in Dutch, *Waddenzee*) which is listed on UNESCO's World Heritage List. We will embark on a big shrimp trawler and sail the waters of this shallow sea. During our trip, the trawler catches our evening diner: Saturday night we will eat fresh shrimp! If we are lucky we might catch as well a glimpse of the many seals in the Wadden Sea!

Conference venue

The conference will be held at the Stayokay Hostel in Egmond, located in the countryside, in the Kennemer Dunes, a 30 minute walk away from the center of Egmond-aan-Zee and the beach.

The conference room at the Hostel has all facilities essential for a modern day lecture room (beamer, projection screen, curtains for darkening, air-conditioned and air-controlled). A nearby smaller conference room will be used as poster area.

All rooms at the Hostel offer basic facilities with shower/toilet. Breakfast, lunch and diner will be served at the Hostel dining room for full-board participants. The Hostel offers free WiFi to all participants in the lounge area, the conference rooms, and the bar. (There is no WiFi available in the rooms, however.) Active participants can also hire a bike and explore the beautiful surroundings of the Hostel.

Figure 3 – Stayokay Hostel in Egmond.

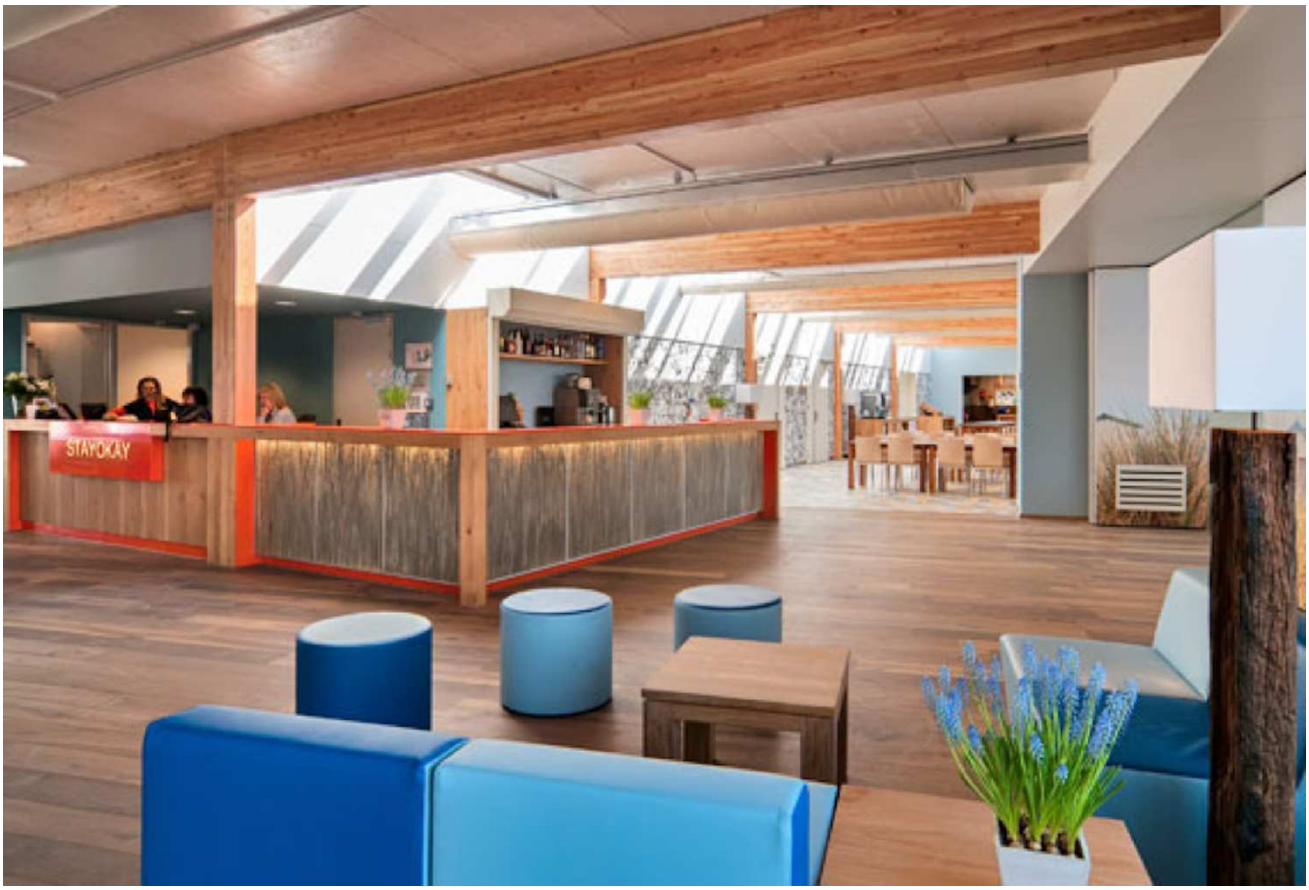

Figure 4 – Interior of the Stayokay Hostel.

Accommodation

The default for full-board-participants is accommodation in 4-person rooms at the Stayokay Hostel in Egmond. The Hostel was fully refurbished in 2012 and is now one of Stayokay's most aesthetically appealing venues. The relaxed atmosphere, cozy bar, well-equipped meeting room, sun-dressed terraces, and numerous options for children and sports make this hostel a perfect choice. The meals are rated excellent and are prepared using mainly fair trade and organic ingredients.

In addition to the 4-person rooms, there are a limited number of single and double rooms available, which will be assigned on a first-come, first-served basis, at an extra cost (see "Registration and payment").

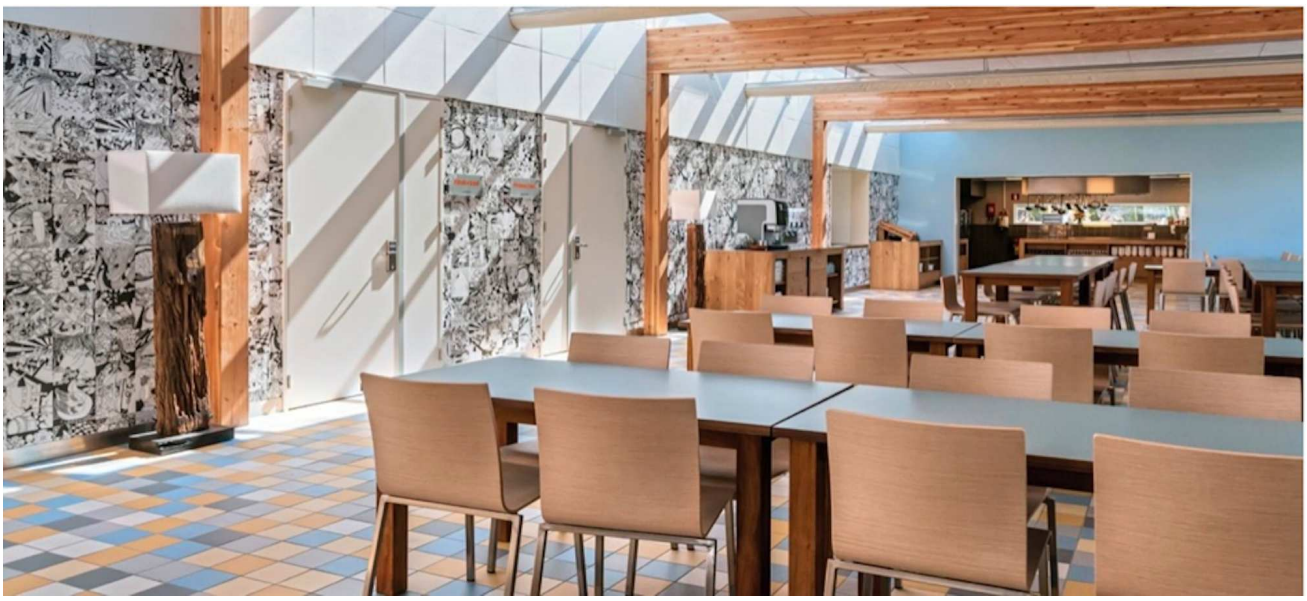

Figure 5 – Dining room.

Participants who want to come earlier or stay longer can reserve extra nights at the Stayokay Hostel. They can choose between single, double, or 4-person rooms, and reservations include breakfast. Lunch and dinner before and/or after the conference are optional and have to be ordered on site. Extra nights cannot be reserved on the IMC registration form and must be booked via the website of the venue.

Participants who do not want to stay at the Stayokay Hostel can contact the Local Organizing Committee (LOC) for alternative accommodation. In that case, the LOC will act as an intermediate only.

Program and social events

Program. The IMC LOC welcomes the arriving participants on Thursday afternoon, June 2nd. In the evening, we will have our first dinner and a welcome session. The Friday program consists of lectures and the IMO General Assembly Meeting. The Saturday program offers lectures, the excursion to the Wadden Sea, dinner, and evening entertainment. On Sunday morning, we continue with the lecture sessions, until 13^{h}, when the conference closes.

Lectures and posters. Lectures will have a duration minimum 10 and maximum 30 minutes, with the actual length depending on the total amount of contributors. Each lecture must allow 2–3 minutes for questions and comments.

Posters are welcomed and offer an opportunity to present special topics not suitable for a lecture. Also, participants wanting to share their results but not willing to give a lecture are welcome to present a poster.

Proceedings. All contributions to the conference, both lectures and posters, should find their way to the IMC 2016 Proceedings, either as a paper or at least as an abstract. Therefore, contributors are strongly advised to have their paper ready before their talk or poster presentation. Articles should be written according to the instructions that will published on the IMC 2016 web pages (see "Information and contact details" at the end of this announcement). A template in Word is available. All papers of the IMC 2016 Proceedings will be registered in the Harvard-NASA Astrophysics Data System.

Scientific Organizing Committee. In order to guarantee the high quality of the program, all lecture and poster abstracts have to be submitted before the IMC and will be supervised by the IMC 2016 Scientific Organizing Committee (SOC). It will compile the conference program and the content of the IMC 2016 Proceedings.

Socializing. It cannot be overemphasized—socializing is one of the main goals of an IMC. Therefore, the conference program will allow ample time for personal contacts, in particular during the opening reception, the breaks, and the Saturday afternoon excursion, and during the evenings at the bar, were you can also play music, so bring your instrument if you have one!

Travel information

Egmond can easily be reached by plane (via Amsterdam Schiphol International Airport, Eindhoven Airport, or Rotterdam Airport), and is well connected to other parts of the Netherlands and the capital Amsterdam by train and bus. The bus stop is right in front of the Stayokay Hostel. Egmond is located very close to the A9 motorway, between Amsterdam and the lovely city of Alkmaar, only 10 km away.

From Amsterdam Schiphol International Airport. At the airport, take the Intercity train in the direction of Lelystad Centrum, and change at Amsterdam Sloterdijk station to the Intercity train in the direction of Alkmaar. Disembark at Castricum station (recommended) or at Alkmaar station. From Castricum station, take bus 164 to the Hostel (stop Rinnegommerlaan). From Alkmaar station, take bus 164 in the direction of Egmond, and get off at the Texaco or Rinnegommerlaan stop.

To plan the train trip from the airport, we recommend to use `http://www.9292.nl`. A single trip from Schiphol to Egmond takes between 1 to 1.5 hours and will cost around 10 EUR.

Traveling by car. If you come from the north, take the A9 motorway in the direction of Alkmaar and then the N9 road towards Den Helder. Next, take the Egmond exit. At the intersection, turn right towards Egmond-Binnen and Castricum. After approximately 250 m, you will see the Stayokay Hostel on your right, next to the staples.

From the south, take the A9 in the direction of Alkmaar. Take exit 10 towards Zaanstad/Uitgeest/Castricum. From Uitgeest, head towards Castricum. After having passed Castricum, continue through Bakkum towards Egmond-aan-de-Hoef. This road leads you to Egmond-Binnen. The Stayokay Hostel is on your right, next to the staples.

Carpooling. Sharing a car with others can help to reduce the number of cars and traveling costs, and stimulates socializing as well. Therefore carpooling is encouraged by the LOC. For privacy reasons, information about the travel plans of participants will not be distributed publically. If you want to share a car with others, inform the LOC and they will bring you in contact with the right person.

Parking. You can park your car for free next to the Hostel.

Transfer to Meteoroids. After the closing of the conference, a free shuttle service will be provided to Noordwijk for those participants who will also participate in the Meteoroids 2016 Conference and have indicated on their registration form that they want to make use of this service.

Figure 6 – Connections to the IMC 2016 location.

Registration and payment

The standard registration fee is 175 EUR for those registering no later than February 28, 2016, and 205 EUR, for those registering between March 1 and April 15, 2016, after which date registration will be closed. Mind that registration may be closed earlier if full capacity is reached before the deadline!

The standard registration fee includes 3 nights of accommodation in a 4-person room (June 2 until June 5) at the Stayokay Hostel, in full board from Thursday evening till Sunday noon (hence, including breakfast, lunch, and diner, except for (alcoholic) beverages), all IMC lectures and the poster session, coffee breaks, the excursion to the Wadden Sea and the Saturday evening program, conference materials, and the digital IMC 2016 proceedings. An IMC 2016 T-shirt and printed IMC 2016 proceedings can be ordered upon registration at an extra cost of 10 EUR and 15 EUR, respectively.

In addition to the 4-person rooms, there are a limited number of single and double rooms available, which will be assigned on a first-come, first-served basis. The registration fee for double and single rooms are 250 EUR and 350 EUR per person, respectively, until February 28, and 30 EUR more after that date.

Participants arranging their own accommodation are charged 100 EUR until February 28 and 130 EUR after that date. They enjoy the same benefits as the other participants, except for accommodation and breakfast.

The cancellation policy is as follows:

- until February 28, 2016: full reimbursement, reduced with a cancellation fee of 15 EUR;
- between March 1 and April 15, 2016 : partial reimbursement of half of the total fee paid;
- from April 16, 2016 onward: no reimbursement.

To register, please visit the IMC 2016 web pages (see below under “Information and contact details”). There, you will also find useful information on how to pay the registration fee. **Notice that payment is due upon registration!**

Information and contact details

For further information, updates, latest details, registration, and payment, please check the IMC 2016 web pages regularly at `http://imc2016.imo.net`. Alternatively, click on the IMC 2016 logo at the IMO website home page, `http://www.imo.net`, which will redirect you the IMC 2016 web pages. All inquiries about the IMC 2016 and/or your registration should be made via email to `imo2016@imo.net`. The IMC 2016 also has a Facebook page which you can access via the Facebook button on the IMC 2016 web pages.

From the Treasurer — IMO Membership/WGN Subscription Renewal for 2016

Marc Gyssens

We invite all our members/subscribers to renew for 2016. The fees are as tabulated below. We are happy that we can offer WGN at the same cost as last year. We also continue to offer an electronic-only subscription at a reduced rate.

IMO Membership/WGN Subscription 2016				
Electronic + paper with surface mail delivery:		€26		US$ 39
Electronic + paper with airmail delivery (outside Europe only):		€49		US$ 69
Electronic only:		€21		US$ 29
Supporting membership:	add	€26	add	US$ 39

It is possible to renew for two years by paying double the amount.

General payment instructions can be found on the IMO's website, at `http://www.imo.net/payment`. Members and subscribers who have not yet renewed will find enclosed a leaflet where these payment instructions are further detailed. Please follow these instructions! Choosing the most appropriate payment method results in low or even no additional costs for you as well as the IMO. The IMO strives to keeping these costs low in order to control the price of the journal!

When you renew, give a few minutes of thought to becoming a **supporting member**. As you may know, there is an IMO Support Fund. With this Support Fund, we support to meteor-related projects. Our ability to provide this service to the meteor community depends primarily on the gifts we receive from supporting members!

Another way to help meteor workers with limited funds is to offer them a gift subscription.

We already thank all our members that will renew for their continued trust in our Organization!

One final request: every year, a lot of members renew late. As a consequence, back issues that already appeared have to be sent out to these members. Please support our volunteers in their bimonthly effort to have WGN shipped to you by renewing promptly! Thank you for your understanding and cooperation!

IMO bibcode WGN-435-gyssens-renewals NASA-ADS bibcode 2015JIMO...43..126G

Meteor Science

What do we see as ANT, Apex and Toroidal sources? — What meteors are, where meteors came from, where meteoroids are going.

Masahiro Koseki[1]

We found that the observabilities of meteors depend strongly on meteor velocity; the ratio of the number of CCD to photographic meteors is expressed as a quadratic function of the velocity, and the observability for radar observations has a clear peak around V_g=30 km/s. If we do not compensate for the observability, we are under the impression that radar observations contribute most to the Toroidal activity, CCD observations record a huge number of the Apex meteors, and photographic meteors concentrate on the ANT area. We assume that the observed number against the velocity shows roughly the observability for each observational technique and get more plausible results: in first place in radar observations is the Apex source and in optical observations ANT, while the Toroidal source is not so impressive.
We calculated the radiants of 3212 comets and 1533 PHAs (potentially hazardous asteroids), finding 193 radiants of periodic comets, 1013 radiants of non-periodic comets and 3018 radiants of PHAs. Comparison of predicted to observed radiants reveals a very interesting fact: the contribution of the periodic comets to sporadic meteor activities is small, though we have clear recollections of meteor showers made up by a substantial number of massive meteoroids. It is clear many meteoroids from periodic comets meet Earth with low velocity and do not radiate enough light to be visible. Both predicted and observed radiant distributions clearly separate into two regions except for radiant areas relating to periodic comets. It is suggested that the Apex source is descended from non-periodic comets, ANT from asteroid kinsfolk and the Toroidal source is accumulated by older particles near Earth's orbit from both comets and asteroids.

Received 2015 July 28

1 Introduction: Historical review

Visual observers have noticed the Apex source as the meteor numbers rising toward morning twilight and the ANT (antihelion) source as the ecliptic activities. Olivier (1960) collected many visual observations and compiled tables of meteor hourly rates day by day and from hour to hour. Figure 1 is compiled from his December data and the increase in meteor numbers shows the Apex source meteor activity. We think this increase comes from a geometrical effect, that is, the Earth sweeps up more meteoroids on its front side than to the rear.

On the other hand, we need to know a 'radiant point' in order to recognize the ANT source, though a single observer can only record meteor paths not each radiant. The definition of 'a radiant' in visual observations (Koseki, 2014) leads naturally to heaps of radiants at any major shower. If we exclude them, we might notice an 'accidental' or 'chance' radiant distribution. Figure 2 shows the radiant distribution in ecliptic $(\lambda\text{–}\lambda_\odot, \beta)$ coordinates of visual observations by NMS (the Nippon Meteor Society). It makes clear the concentrations of radiants around the Apex source and the ANT in addition to those of major showers. Five circles (distorted by Hammer Projection) in this figure drawn with 30° radii centered at $(\lambda\text{–}\lambda_\odot, \beta)$=(270,0), (340,0), (200,0), (270,65) and (270,−65) represent the five radiant concentration areas (see below).

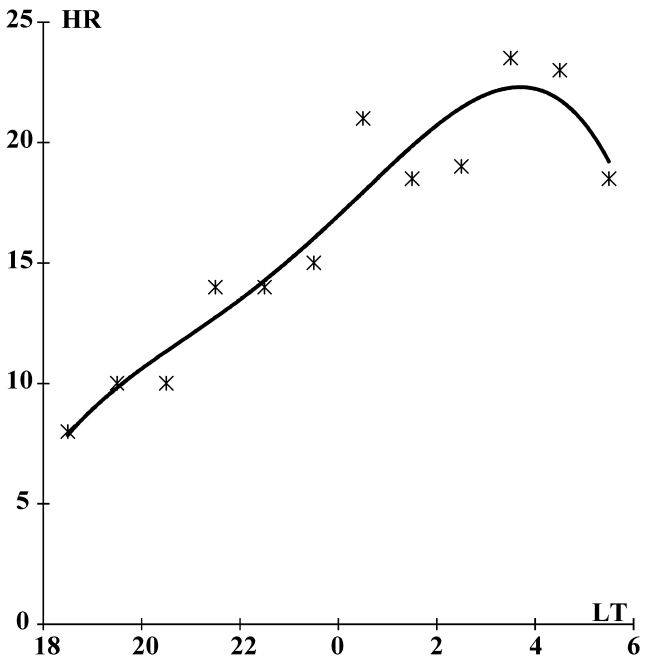

Figure 1 – Mean change of hourly meteor numbers compiled from Olivier's December data (LT: local time).

The 1940's military radar operations developed into modern meteor observations in daytime and found many echoes shooting from around the Sun, the Helion source. This daytime meteor activity is a difficult target for optical observations, though enthusiastic observers caught some meteors from daytime showers. The 1950's photographic observations showed an analogous scenario to visual ones; prominent shower activities, abundant Apex meteors, and rich ANT meteors also.

[1]The Nippon Meteor Society (NMS), 4-3-5 Annaka, Annaka-shi, Gunma-ken, 379-0116 Japan. Email: geh04301@nifty.ne.jp

IMO bibcode WGN-435-koseki-what
NASA-ADS bibcode 2015JIMO...43..127K

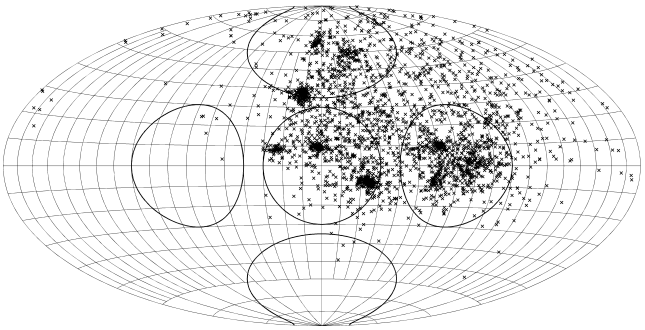

Figure 2 – Radiant distribution in $(\lambda–\lambda_\odot, \beta)$ coordinates of visual observations by NMS. Center of plot at $(\lambda–\lambda_\odot, \beta)=(270,0)$.

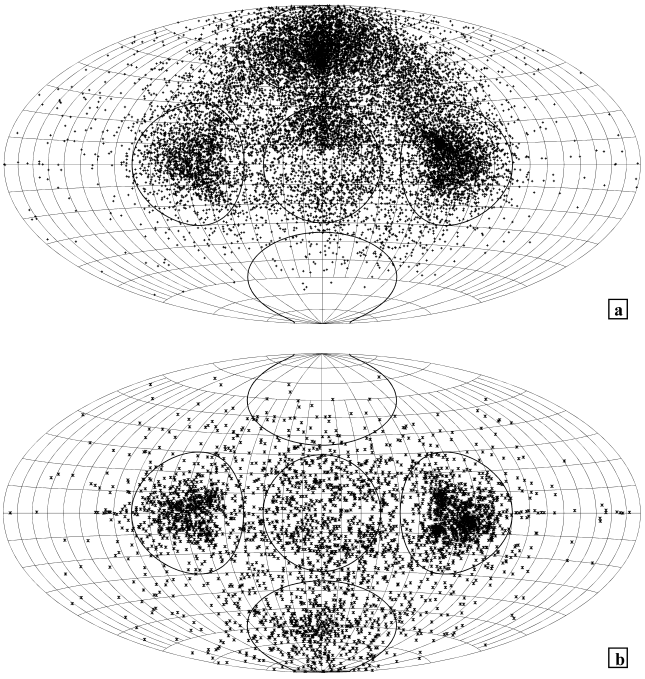

Figure 3 – Radiant distribution in $(\lambda–\lambda_\odot, \beta)$ coordinates of (a) Harvard radar data in 1961–65; (b) Adelaide radar data in 1960–61 and 1968–69.
Data at `http://sbn.psi.edu/pds/asteroid/EAR_A_VARGBDET_5_METORB_V1_0/data/` .

The 1960's radar observations revealed additional meteor source(s) and Hawkins (1963) named this source as 'Toroidal' by its spatial form. The Toroidal source was recognized firstly at high ecliptic latitude from the northern hemisphere and also at high southern ecliptic latitude later; for examples see Figure 3a and 3b. The Toroidal source(s) became a wonder for meteor researchers. The Toroidal sources are unique and we study the difference between Toroidal source(s) and others later (sections 3.2.3 and 4.1). We now have four sources of meteors on the heavens; Apex, Helion, ANT, and Toroidal sources, abbreviated AHAT (a hat) hereafter.

It is said there are six sources of meteors: ANT, Helion, north and south Toroidal, and north and south Apex. As ANT and Helion sources have a common origin, so the two Toroidal branches have similar ancestors, as do the two Apex branches (see section 3.1.3). Here we study ANT, north Toroidal as representative, and north and south Apex together.

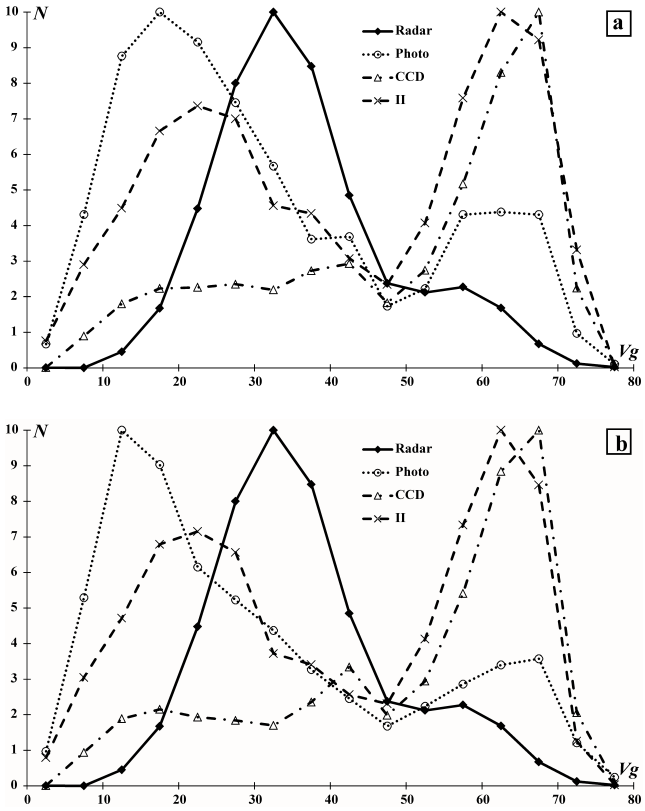

Figure 4 – Comparison of geocentric velocity distributions for different observational techniques (a) using original shower classification; (b) using shower classification revised by Table 1. Standardized to 10 at maximum.

2 What meteors are

2.1 Different observability depending on technique

Koseki (2014) showed various meteor scenes resulting with different observational techniques, from the view of the magnitude range recordable by the various techniques. Meteor magnitude plays an important role in observational selectivity but geocentric velocity of meteors works as a critical condition also. We cannot regard raw observational data as giving us real figures of meteoric phenomena. Figure 4a plots the geocentric velocity distribution of 'sporadic' meteors standardizing the maximum number to 10 and shows a 'favorite' velocity for four observational techniques; radar (19317 orbits observed 1961–65, (Lindblad & Steel, 1994)), image-intensifier (II, 3834 orbits, (Shigeno & Yamamoto, 2012)), photographic (4451 orbits, Table 6 of (Koseki, 2009)), and CCD (26514 orbits observed in 2013, (SonotaCo, 2014)). We call them simply radar, II, photo, and CCD for conciseness. Radar observation has a single peak around $V_g = 30$ km/s. II shows bimodal peaks with $V_g = 20$ and $V_g = 60$ km/s. Photo meteors resemble II but contrary to II the peak at $V_g = 20$ km/s is the primary one. CCD has an extremely sharp peak near $V_g = 70$ km/s, though CCD as well as II observations are both called video observations.

It is not proper to think such differences necessarily come from the difference of meteoroid characteristics of each observation. It is necessary to check whether the 'sporadic' classification of each study affects the results,

Table 1 – Major and important minor meteor showers selected from IAUMDC (2015), which we exclude for selecting sporadic meteors.

IAU-No.	α	δ	λ–$\lambda_\odot$	β	V_g	e	q	i	ω	Ω	$\lambda_\odot$	Stream
1	306.6	−8.2	179.9	10.7	22.2	0.770	0.602	7.7	266.7	128.9	127.0	CAP
2	49.4	13.0	186.5	−5.0	28.0	0.830	0.352	5.4	115.4	37.3	224.0	STA
4	113.2	32.5	207.7	10.6	34.6	0.897	0.141	24.0	324.4	261.5	262.1	GEM
5	342.1	−15.4	212.0	−7.2	40.5	0.972	0.087	26.4	148.9	312.2	125.6	SDA
6	272.0	33.3	240.6	56.7	46.6	0.980	0.921	79.6	214.3	31.8	32.4	LYR
7	48.3	58.0	283.1	38.3	59.4	0.987	0.953	113.2	151.3	140.2	140.2	PER
8	94.7	15.9	246.0	−7.5	66.5	0.968	0.578	164.3	81.5	28.7	208.6	ORI
10	230.0	49.5	277.0	63.6	41.4	0.688	0.979	72.0	172.0	283.3	283.3	QUA
11	182.1	2.6	186.9	3.2	29.2	0.851	0.382	3.5	349.1	280.5	354.0	EVI
12	284.0	52.7	158.1	74.5	24.0	0.808	0.984	35.9	201.4	139.4	145.2	KCG
13	154.2	21.6	273.2	10.2	70.7	0.902	0.985	162.4	173.5	236.2	235.1	LEO
15	219.4	75.3	218.5	72.1	33.0	0.796	0.944	51.5	204.9	270.7	271.0	URS
16	131.9	0.2	228.8	−17.0	58.0	0.982	0.224	124.9	124.0	84.8	265.5	HYD
17	58.6	21.6	197.0	1.3	28.3	0.835	0.350	3.1	294.9	226.2	224.0	NTA
19	101.8	8.1	201.2	−14.8	42.0	0.996	0.193	35.2	128.1	80.2	260.9	MON
20	175.2	22.2	252.5	18.4	63.7	0.962	0.541	139.4	265.0	283.3	274.0	COM
22	159.5	36.7	297.6	25.9	61.9	0.998	0.616	125.3	102.7	208.4	209.0	LMI
23	101.6	26.7	254.4	3.7	68.8	0.927	0.731	172.9	241.7	209.0	206.0	EGE
26	344.7	0.4	222.7	6.4	40.5	0.972	0.071	23.0	332.6	139.0	123.4	NDA
31	336.9	−1.5	291.2	7.6	65.9	0.964	0.581	163.9	97.9	44.4	46.9	ETA
32	156.1	32.7	243.2	21.1	62.3	0.953	0.554	133.8	265.6	262.2	262.4	DLM
208	50.2	39.4	248.2	20.3	64.5	0.976	0.742	138.9	241.9	171.3	170.0	SPE

because Figure 4a is drawn on the basis of each study's original definition for the classification. We decided instead to exclude 'shower' meteors listed in Table 1 and to use the results as a uniform data set hereafter.

We take the discrimination level as $D(A,B) < 0.4$ by Southworth & Hawkins' (1963) criterion:

$$[D(A,B)]^2 = (e_A+e_B)^2 + (q_A-q_B)^2 + \left(2\sin\frac{I_{AB}}{2}\right)^2 + \left[\frac{1}{2}(e_A+e_B)\,2\sin\frac{\Pi_{AB}}{2}\right]^2$$

If we select shower members to investigate a meteor shower, this condition is too wide. But because there are several meteors possibly recorded with erroneous velocity, especially of high speed such as Perseids and Orionids, we should securely exclude shower meteors in order to study 'sporadic' meteors. It is necessary to apply such an apparently exaggerated limit to get rid of the influence of shower meteors.

Table 2 lists the resulting percentages of shower meteors except for radar ones. We do not exclude any shower members from radar data, because shower orbits of radar meteors are somewhat different from optical data and, moreover, the contribution of radar shower meteors to the whole volume is small enough for this study. We include major showers, Geminids (GEM) and Taurids (STA and NTA) as sporadics, but this ignorance does not result in a huge number of radar ANT (see Table 3 later). We omit meteor showers in Table 1 for optical (II, photo and CCD) observations in selecting sporadic meteors. This causes no essential discrepancy between the former result (Figure 4a) and 'sporadic' data revised by Table 1 (Figure 4b).

Table 2 – Percentages of orbits classified as given shower members using $D(A,B) < 0.4$. There are some meteors counted doubly or triply, because there is a twin shower, Orionids (ORI) and η-Aquariids (ETA), and several other showers also have similar orbits.

IAU-No.	Stream	Photo	CCD	II
1	CAP	3.15	0.72	3.16
2	STA	5.14	2.84	2.35
4	GEM	4.07	12.84	6.89
5	SDA	1.21	0.47	2.97
6	LYR	0.34	0.80	0.10
7	PER	10.00	7.22	4.20
8	ORI	2.04	4.24	2.58
10	QUA	0.81	1.58	1.30
11	EVI	3.64	1.81	2.45
12	KCG	1.69	0.45	0.29
13	LEO	0.76	2.41	4.43
15	URS	0.18	0.35	0.39
16	HYD	0.31	1.73	0.50
17	NTA	4.49	3.14	3.10
19	MON	0.56	1.54	0.89
20	COM	0.40	1.54	0.68
22	LMI	0.16	0.09	0.18
23	EGE	0.52	1.11	0.78
26	NDA	0.63	0.38	0.86
31	ETA	2.00	4.17	2.74
32	DLM	0.34	1.53	0.60
208	SPE	0.25	0.67	0.05

We note the contributions of 'major' showers (e.g., GEM and PER) are large naturally and the ecliptic showers (e.g., STA and NTA) are the next. The applied limit $D(A,B) < 0.4$ seems to be too large for slower

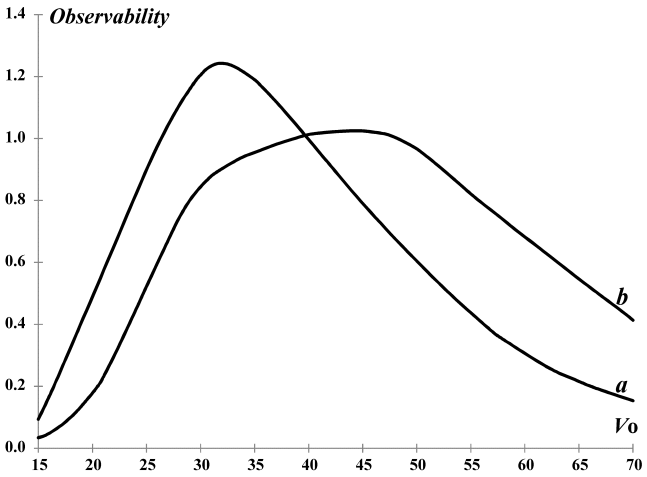

Figure 5 – Observability function for radar observation (from Kasheev et al., 1967). Line a for high sensitivity system which can recognize 10^{10} electron/cm echoes and b for low sensitivity system (2×10^{11} electron/cm). They standardized the observability to unity at 40 km/s. Two other lines between high and low electron density are omitted here.

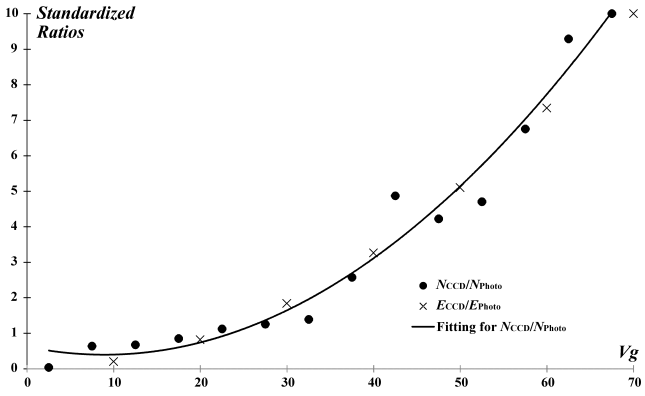

Figure 6 – Comparison of observability dependence on velocity between photographic and CCD observations. Ratios are standardized to 10 at the maximum. Black circles: the ratios of observed velocity distribution of CCD meteors to photo with best fitting smooth curve. Crosses: standardized estimation using formulae in text.

meteor showers, that is, the ecliptic ones, because the observed error in velocity determination rises with the velocity. Though we may have excluded some possible ANT meteors classifying as shower meteors, the favorite velocities remain in the plots (Figure 4a and 4b). It is, therefore, suggested that each observational technique favors its own unique velocity, that is, the obtained data are biased by every technique.

2.1.1 Restriction in radar observations

Kasheev et al. (1967) gave observability functions for radar observation (see Figure 5). Observability changes with the detection level of the line density of electrons, as shown by lines a and b in Figure 5. They explained: "The ionization coefficient of slow meteors is small and the initial radius of ionized trail increases in case of swift meteors. The more sensitive instruments we use, the smaller meteoroids we can record. The initial radius of the train of smaller meteoroids is larger, because such meteoroids begin evaporating at higher altitude. Then the sensitive implements can record less number of fast meteors." Line a resembles the velocity distribution of the Harvard radar results (see Figure 4b). It is suggested the Harvard velocity distribution is caused by its observability.

2.1.2 Strong bias in optical observations

We can explain the difference in velocity distribution between optical observational techniques also. It is easy to understand that faster meteors are brighter and more observable than slower ones when their masses are the same. But, why is the detectability bimodal for photo and II though CCD records predominantly brighter meteors? It can be explained by the difference of camera lenses especially by its focal length. CCD observations started as fireball surveys and use camera lenses of very short focal length, such as $f = 6$ mm. In contrast, other optical observations used longer lenses than CCD in order to determine exact meteor paths and orbits.

McKinley (1961) gave the empirical formula of the efficiency E of a meteor camera:

$$E = k\frac{a^2 A_s}{(1+x)f^n}$$

where k includes the effects of lens quality and light loss, a is lens aperture, f the focal length, A_s the area covered in the sky by the camera, and x the closed-open ratio for a rotating shutter. He stated the exponent n is probably near unity but may be as high as 2. If we compare a typical CCD lens of $f = 6$ mm, $F\ (= f/a) = 0.8$, and $A_s = 56 \times 43°$ with a usual film camera lens of $f = 50$ mm, $F = 1.4$, and $A_s = 24 \times 36°$, in the case where $x = 0$, $n = 1$ and k is equal, the film camera efficiency and that of the CCD are nearly equal. But this does not agree with our experiences. When we can record 1 meteor an hour by CCD, a film camera needs roughly 10 hours or more for a meteor.

It seems to be natural the exponent n might be larger than unity especially for CCD, because the angular velocity on the pixels becomes smaller with the shorter focal length. A photosensor or a film can receive light per pixel (i.e. per unit square) in proportion inversely to the square of $F\ (= f/a)$ and to the angular velocity of meteors, which can be replaced by their geocentric velocity V_g and, therefore, f as $V_g \times f$. So we can rewrite the above formula as follows:

$$E = k\frac{A_s}{(1+x)F^2 V_g f} = k\frac{a^2 A_s}{(1+x)f^3 V_g}$$

But, it is very interesting that the ratios of velocity distribution of CCD to photo meteors vary in proportion to the square of velocity (Figure 6). It is suggested the efficiency differs in CCD and in photo. We can expect the efficiencies for these two devices:

$$E_{\mathrm{CCD}} = k\frac{A_s}{(1+x)fF^2} \qquad E_{\mathrm{photo}} = k'\frac{A_s}{(1+x)V_g^2 fF^2}$$

Here we adopt $k' = 28.4$ in order to give $E_{\mathrm{photo}} = 0.1$ at $V_g = 50$ which represents approximately hourly photographed meteor rates and $k = 1.59 \times 10^{-3}$ in order to

normalize them, because these efficiencies are the relative values in each measurement. The estimated ratios $E_{\rm CCD}/E_{\rm photo}$ standardized to 10 at the maximum are given as crosses in Figure 6 and are in good agreement with observations. It is very clear that the observability in optical observations strongly depends on meteor velocity, analogously to radar observations. But k is not equal in the two techniques, because CCD is highly sensitive compared to ordinary films.

2.1.3 The approximate dependence of observability on the velocity of meteors

The velocity distribution of radar meteors looks like the observability function (line a) by Kasheev et al. (1967) as shown in section 2.1.1 and this suggests the true distribution may be uniform over the range. We have confirmed that optical observations are hindered by their restrictions also. Though whether the velocity distribution is uniform is uncertain, we may consider it may be true for optical meteors and had better check this idea.

Figure 7a shows the distribution of observed radiant density at each 10° from the Apex instead of plotting the whole sky in Hammer projection as in Figure 3a and 3b. The density of radiants in video observations (both CCD and II) shows a tendency to decrease with the Apex elongation, though the characteristics of both are considerably different (see Figure 4a and 4b). Radar observation shows a unique distribution; the peak around 60° results from the Toroidal source. Photographic observation, which we have considered is a standard technique and gives a general result, shows another unique distribution. It has two peaks; one is the Apex source and the other is the ANT.

If we regard the difference in meteor velocity (Figure 4b) as the observational bias, the difference in radiant distribution shown in Figure 7a seems to be apparent. If we assume the observability is proportional to the velocity distribution as suggested above, we can redraw the observability using moving mean 3 km/s bins (Figure 8; cf. Figure 4b but in Figure 8 we interpret the curves as representing the observability and also the bin size of the calculation is set narrower in Figure 8). The corrected radiant distributions of all four observational techniques become similar (Figure 7b). Is the difference in velocity distribution a real or biased result? We cannot answer this question exactly, because different techniques can detect different 'meteoroids'. But it is very probable that different observations favor each preferred velocity, as we see radar results are affected strongly by meteor velocity.

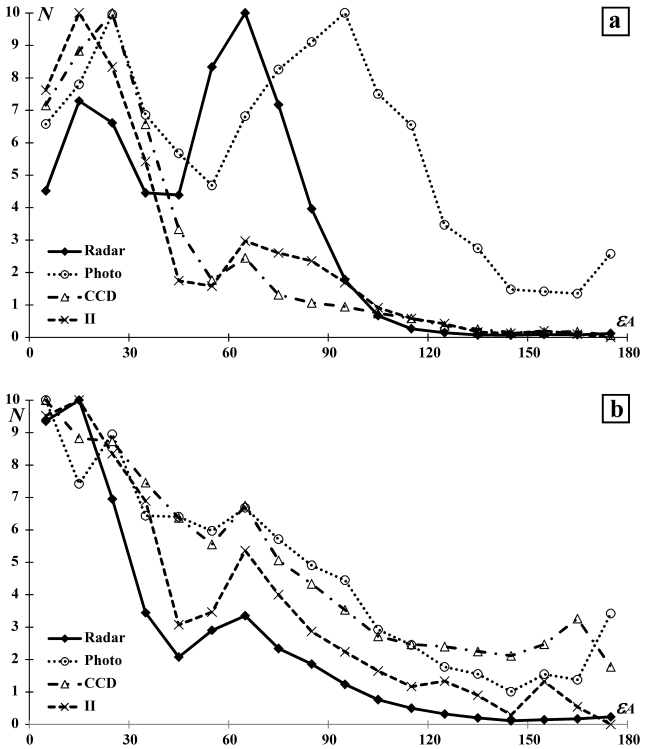

Figure 7 – (a) Variation in radiant density with the elongation from the Apex. (b) Distribution revised by the observability's dependence on the velocity. Standardized to 10 at maximum.

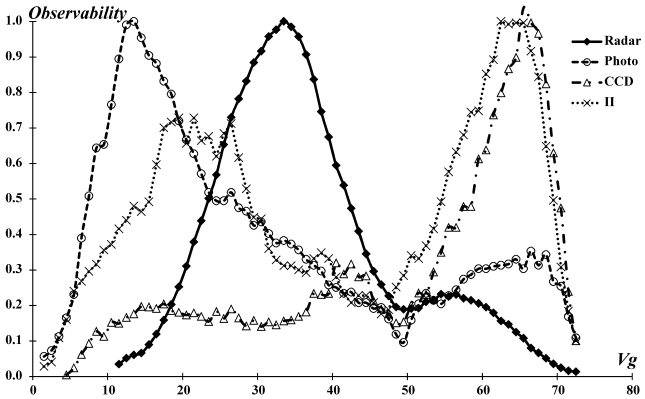

Figure 8 – The observability function using moving mean 3 km/s bins of the velocity distribution.

2.2 What kind of meteors we can see

Figures 7a and 7b showed the observability functions might give plausible results for the radiant distribution. These two figures are standardized to 10 at the maximum and do not show the difference of the radiant density on the celestial sphere between three sources: the Apex, the Toroidal, and the ANT. Figures 9–11 give the radiant density in 10° bins corrected by the areas and standardized by each revised total radiant number. For example, Figure 9a shows radar radiants concentrate around $\varepsilon_A = 60°$, as shown in Figure 7a, and the ratio is about 3, that is, the ANT radiants are three times denser than the surrounding. Figure 9b is similar to Figure 9a but this is revised by the observability function (Figure 8). The revised radar curve rises to over 5 of the ratio near the Apex and become analogous to tendencies of other observations. Figures 10a and 10b are drawn for the Toroidal and Figures 11a and 11b for the ANT, and each b figure represents the revised ones. All three b figures suggest the observability function on the velocity is effective for a first approximation to get the true radiant distribution.

We would have thought CCD observations see the Apex meteors as the strongest source, photo the ANT ones, and radar the Toroidal ones (see the left part of Table 3). Table 3 summarizes Figures 9–11 and shows the effect of the observability function. The Toroidal

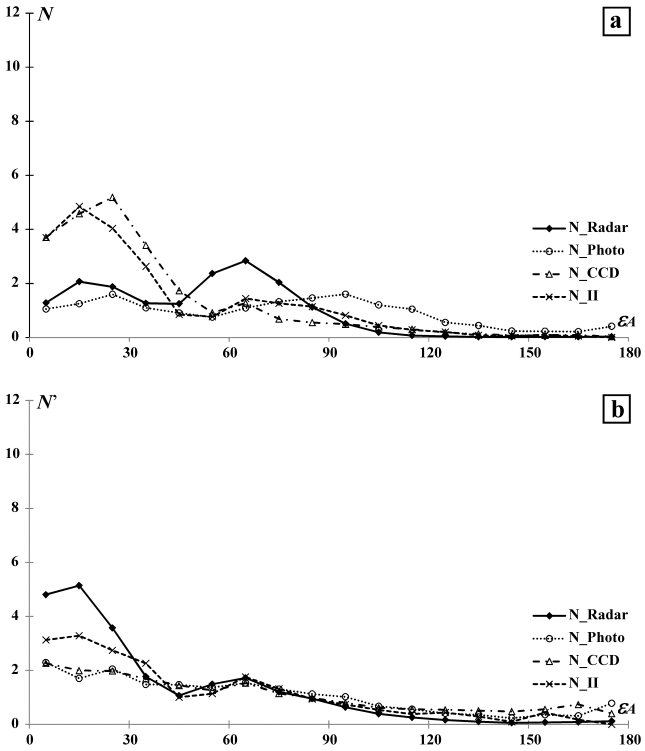

Figure 9 – Radiant density as a function of elongation from the Apex. (a) Original. (b) Revised by the observability function.

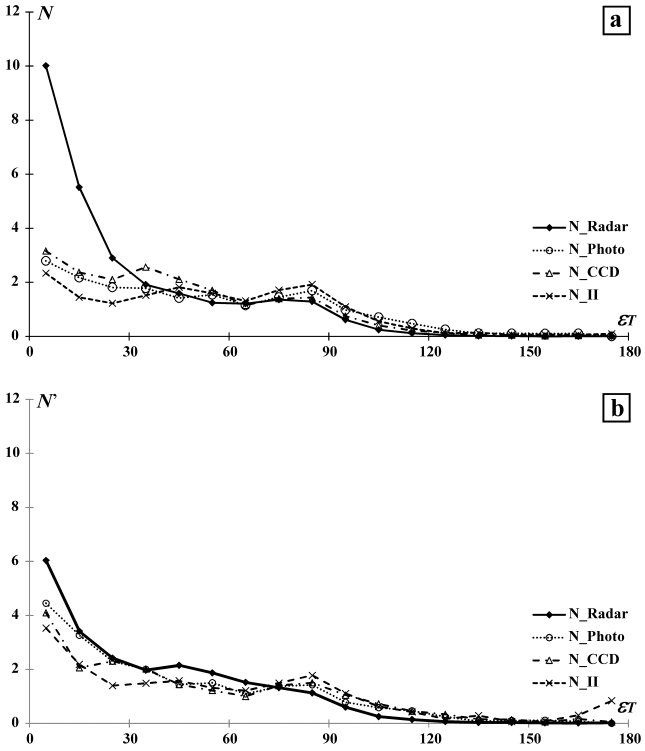

Figure 10 – Radiant density as a function of elongation from the center of the Toroidal region. (a) Original. (b) Revised by the observability function.

source recedes from the first place in radar observations and the Apex source weakens in CCD observations to last place (see the right part of Table 3).

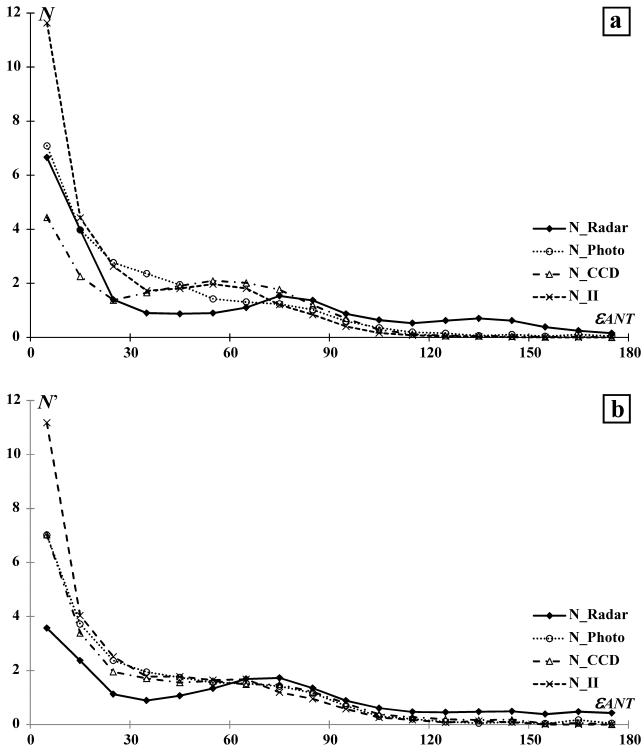

Figure 11 – Radiant density as a function of elongation from the ANT radiant. (a) Original. (b) Revised by the observability function.

3 Where meteors came from: Possible origin of meteors

3.1 Calculation of radiant points from comets and asteroids

We have long been under the impression that a comet bears meteors. October Draconids bear the name of their parent body and are called Giacobinids, and Andromedids are called Bielids. Though the parent comet of some major showers and of course of many minor showers is still unknown and the searches are widened to 'asteroids', we think vaguely that those asteroids are extinct or exhausted comets. It seems proper to study whether comets or asteroids are the parent bodies of sporadic meteors. We calculate possible meteor radiants on the basis of comets and asteroids, and compare them with observations.

3.1.1 Calculation method

There are many methods to predict meteor radiants from interplanetary bodies. They are orbiting around the Sun without colliding with Earth, that is, their orbits do not intersect with the Earth's orbit. Therefore, we convert their orbits to appropriate orbits to produce meteor activity on Earth. Here, we adopt Koseki's (2012) hypothesis:

1. The axis of the meteoroid orbit remains the same as the parent body.

2. The size of the meteoroid orbit, i.e. the semi-major axis, is kept the same.

Condition 1 means that we assume the fourth term in Southworth-Hawkins' criterion (section 2.1) is zero.

Table 3 – The percentages of all meteors within 30° of each source. The left part of the table refers to the real observed number and the right part is revised by considering the velocity dependence in observations. Apex: $(\lambda\text{–}\lambda_\odot, \beta)$=(270,0). Toroidal: $(\lambda\text{–}\lambda_\odot, \beta)$=(270,65). ANT: $(\lambda\text{–}\lambda_\odot, \beta)$=(200,0).

	Observed					Corrected				
	Photo	Radar	CCD	II	Average	Photo	Radar	CCD	II	Average
Apex	9.5	12.5	32.2	28.6	20.7	13.1	28.4	13.5	19.9	18.7
Toroidal	13.7	30.7	15.5	9.5	17.4	19.2	21.2	18.0	12.8	17.8
ANT	24.5	19.1	13.5	28.5	21.4	22.4	12.2	19.0	26.8	20.1

Table 4 – Examples of modification of orbits and corresponding radiants. λ_Π and β_Π represent the perihelion direction in ecliptic coordinates.

Name	e	q	i	ω	Ω	a	λ_Π	β_Π	α	δ	V_g	$\lambda_\odot$	$\lambda\text{–}\lambda_\odot$	β	$D_{\rm SH}$
1P/Halley	0.967	0.586	162.3	111.3	58.4	17.8	306.1	16.5							
η-Aquariids	0.966	0.605	163.2	100.6	47.2				338.6	−0.3	66.1	47.2	292.9	8.1	0.047
Orionids	0.969	0.545	163.5	85.4	31.3				96.9	15.6	66.2	211.3	245.4	−7.7	0.107
3200 Phaethon	0.890	0.140	22.2	322.1	265.3	1.27	229.5	−13.4							
DSX	0.794	0.262	18.2	228.0	3.0				158.0	−4.5	28.8	183.0	338.4	−12.8	0.401
GEM	0.881	0.151	23.2	323.9	263.4				115.3	32.5	33.4	263.4	208.1	11.0	0.020

We rotate the orbital plane around the semi-major axis and change its eccentricity and perihelion distance in order to intersect with the Earth's orbit, making this calculation for a series of points all round the Earth's orbit. The calculation starts from the solar longitude 0.0° with 0.1° steps and continues to 359.9°. We calculate $D(A, B)$ and the predicted radiant point for every case and, then, we can find easily the minimum $D(A, B)$ and corresponding radiant point. Here, A is the initial orbit (parent body) and B the converted (Earth intersecting) one.

There can be two intersections; for example, Figure 12a shows how $D(A, B)$ between the initial orbit and the converted one of 1P/Halley changes along with the intersect position, i.e., the solar longitude of the possible activities. This curve has two minima $D(A, B)$, hereafter abbreviated $D_{\rm SH}$, and suggests meteor activities occur twice: η-Aquariids and Orionids.

We select the possible candidates of meteor activities when $D_{\rm SH}$ between the initial and converted orbits becomes less than 0.5. This study does not intend to predict individual meteor activity but instead to find possible radiant distributions on the celestial hemisphere. We ordinarily use the limit $D_{\rm SH} < 0.2$ for probable relationships between celestial bodies and meteor activities. Though it seems too large to apply $D_{\rm SH} < 0.5$ for the radiant prediction, there may be a chance that meteor activities arise even at such a large distance. 3200 Phaethon is the most probable candidate for the Geminid (GEM) meteor shower and a possible source for Daytime Sexantids (DSX). Figure 12b shows the circumstances of 3200 Phaethon. The minima occur twice; $\lambda_\odot$=183.°0, $D_{\rm SH}$=0.401 for DSX and $\lambda_\odot$=263.°4, $D_{\rm SH}$=0.020 for GEM. We know strong perturbations change the orbit and the present orbit alone cannot present the complex scenario. If we search 'possible' distribution of radiants, it is adequate to use the limit $D_{\rm SH} < 0.5$. Table 4 shows the examples of these calculations; the original orbit of 1P/Halley and of 3200 Phaethon with modified orbits and their corresponding radiants.

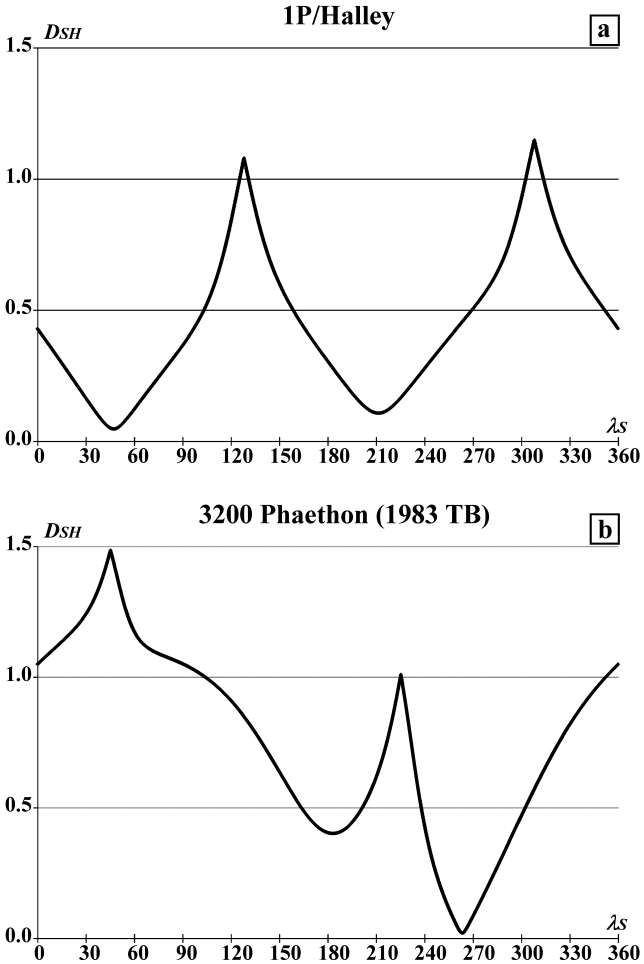

Figure 12 – (a) The change $D(A, B)$ between the initial (A) and converted (B) orbits of 1P/Halley along with the intersect position, i.e., the solar longitude. The minima suggest the two possible activities: $\lambda_\odot$=45° for η-Aquariids, $\lambda_\odot$=210° for Orionids. (b) The circumstances of 3200 Phaethon.

3.1.2 Cometary radiants

3320 orbits are stored (Table 5, downloaded 2015 January 16) in the JPL Small-Body Database (abbreviated SBD hereafter). There are comets split into several nu-

Table 5 – Comet orbits in JPL Small-Body Database (JPL, 2015). Number of split nuclei counts the subordinate bodies.

Comets	Numbered	Denoted			SOHO	Total
		'P'	'D'	'C'		
Registered	383	206	31	1240	1460	3320
Split nuclei	75	2	20	11	0	108
Main body	308	204	11	1229	1460	3212

Use for calculation:
Periodic comets = 308+204+11+2(from SOHO) = 525
Non-periodic comets = 1229+55(from SOHO) = 1284

Table 6 – SOHO comets (classification from (Shanklin, 2015)).

SOHO	Kreutz	Meyer	Marsden	Kracht	Other	Total
	1251	89	32	31	57	1460

clei and some of them are listed individually. We use main body orbits only and, therefore, the total reduces to 3212. 1460 orbits are 'SOHO' and we exclude them from the calculation except for 57 comets classified as 'others' (see Table 6). SOHO comets are almost 'Sun skirting comets' and the 'Kreutz group' is overwhelming. It is proper to reject them in order to avoid misunderstandings by the biased statistics.

It seems to be natural that we divide the remaining comets into two groups: periodic comets and non-periodic comets. We take 308 numbered periodic comets, a further 204 comets denoted 'P', and two additional comets from the SOHO 'other' group. There are 8 comets denoted 'D', i.e. disappeared or dead, among the numbered comets but as they are interesting objects for meteor studies, it is adequate to include them. We should include 11 comets denoted 'D' of periodic nature in unnumbered comets also. We get, therefore, 525 periodic comets for this study. As for non-periodic comets, we add 1229 comets denoted 'C' to the 55 SOHO comets classified 'others' excluding the two periodic ones and we have 1284 non-periodic comets.

We find 193 radiants from periodic comets and 1013 radiants from non-periodic comets using the condition $D_{\rm SH} < 0.5$ (see Table 7). The ratios of the total number of radiants to the number of comets are 0.368 and 0.789 for periodic comets and non-periodic comets respectively. The development of comet observations might explain the difference. The periodic comets discovered recently have larger perihelion distance than those of older comets; such recent comets do not enter within the Earth's orbit. On the contrary, non-periodic comets before the 20th century were discovered when they came near to the Sun and were bright enough for optical observations including by the naked eye; such older comets can come close enough to the Earth to produce a meteor shower.

Figures 13a and 13b show the distribution of calculated radiants in $(\lambda–\lambda_\odot, \beta)$ coordinates for periodic comets and non-periodic comets respectively. We add five radiants of SOHO comets to Figure 13b and their details are shown in Table 8. The Kracht and Marsden

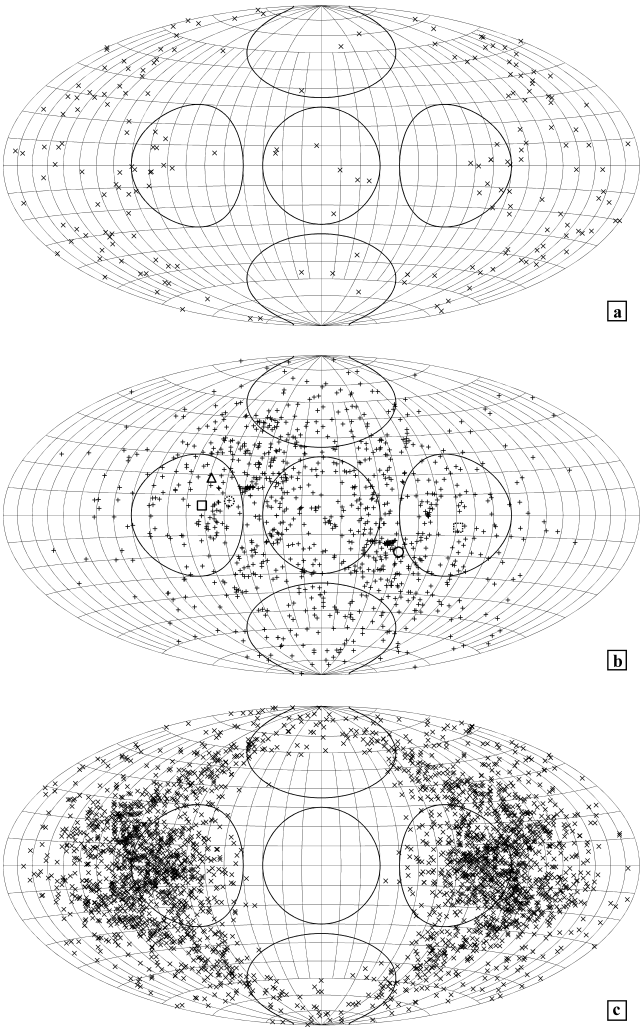

Figure 13 – Distribution of calculated radiants in $(\lambda–\lambda_\odot, \beta)$ coordinates for (a) periodic comets; (b) non-periodic comets; (c) asteroids. Symbols in (b) as follows: Kreutz (C/2007 M6 solid circle, C/2007 X13 dotted circle), Kracht + Marsden (C/2004 J18 dotted box, C/1998 A3 solid box), Meyer (C/2008 F1 solid triangle).

groups might be united into one group, giving three groups in total. We can select the radiant having least $D_{\rm SH}$ from each group. Meyer group comets have only one chance of meteor activity on the Earth; $D_{\rm SH}$ is higher than 0.5 at night time. We selected the closest comets in SOHO and, therefore, some radiants from optically discovered Sun skirting comets are scattered near radiants of the Kreutz group.

Figure 13a amazed us, because the radiant distribution of periodic comets does not show any relation to AHAT. We have long been possessed with the idea that comets are the main origin of meteors. But the greater part of their radiants lies outside AHAT and covers the farthest area from the apex. Visual and other optical observations have not noticed meteor activities in this area, excluding Giacobinids and other exceptional meteor showers.

3.1.3 Asteroidal radiants

We select PHAs (potentially hazardous asteroids) for radiant calculation and 1533 PHAs are stored in SBD (2015 January 16). By the definition of PHAs, their

Table 7 – D_{SH} distribution of cometary and asteroidal radiants.

D_{SH}	<0.05	<0.10	<0.15	<0.20	<0.25	<0.30	<0.35	<0.40	<0.45	<0.50	Total
Periodic comets	19	18	19	19	17	13	18	20	34	16	193
Non-periodic comets	128	108	113	97	100	110	93	107	79	78	1013
Asteroids	1731	476	210	175	133	92	80	54	45	22	3018

Table 8 – Five radiants calculated for Kreutz, Kracht+Marsden, and Meyer groups of SOHO comets, which have the closest orbit to the Earth.

Group	Name	e	q	i	ω	Ω	λ_Π	β_Π	α	δ	V_g	$\lambda_\odot$	λ–$\lambda_\odot$	β	D_{SH}
Kreutz	C/2007 M6	1.000	0.006	124.5	115.2	42.4	272.7	48.3							
		1.000	0.255	121.4	119.0	49.5			97.9	4.7	57.8	229.5	228.8	−18.5	0.262
	C/2007 X13	1.000	0.008	138.3	27.7	306.0	284.5	18.0							
		1.000	0.055	137.7	27.4	305.5			262.7	−16.3	56.1	305.5	317.5	6.9	0.048
Kracht	C/2004 J18	1.000	0.046	11.9	65.3	34.2	99.0	10.8							
+		1.000	0.167	14.6	132.1	326.0			348.5	−11.6	40.3	146.0	198.9	−6.1	0.220
Marsden	C/1998 A3	1.000	0.042	27.4	23.0	80.7	101.4	10.3							
		1.000	0.040	27.3	23.0	80.7			48.7	22.9	46.4	80.7	331.7	4.7	0.002
Meyer	C/2008 F1	1.000	0.032	66.7	46.1	94.6	116.9	41.5							
		1.000	0.153	67.7	45.7	95.7			58.4	39.2	47.3	95.7	328.9	18.5	0.123

minimum orbit intersection distance (MOID) with respect to Earth is less than 0.05 au and absolute magnitude $H < 22$. Though we get many radiants because of the small MOID (see Table 7), the asteroids cannot generate much more meteor showers than comets: it is necessary to note we did not restrict comets to NEC (near Earth comet) and the ratios of radiant bearing comets to total number of comets are less than for asteroids.

Figure 13c shows the calculated radiant distribution. It is very natural that there is no asteroidal radiant in the Apex area and they concentrate in both Helion and ANT areas. Many PHAs intersect the Earth's orbit and give twin radiants. These locate one above the ecliptic and one below it (see Table 4). Therefore, the north or south Helion and the ANT seem to have the same origin. The Apex source and the Toroidal source (section 3.2.1) have north and south branches but we do not need to distinguish north and south branches when we study their origin.

The center of concentrations locates on the far side of both Helion and ANT areas from the Apex. The elongation of the radiants from the Apex increases for non-periodic comets, asteroids, and periodic comets in that order (see also Figure 15 below) and the asteroidal radiants locate nearest to the ANT. If asteroids are the origin of the Helion and ANT meteors, the center should coincide with the observations. We will discuss this problem in section 4.

3.2 The relation of Apex, ANT, Toroidal to comets and asteroids

Figure 14 compares the three ancestral sources by geocentric velocity along with the elongation from the Apex. Meteors from non-periodic comets lie along the parabolic limit, that is, the geocentric velocity of meteors orbiting the Sun on a parabola. Meteors from periodic comets are below the parabolic limit and parallel

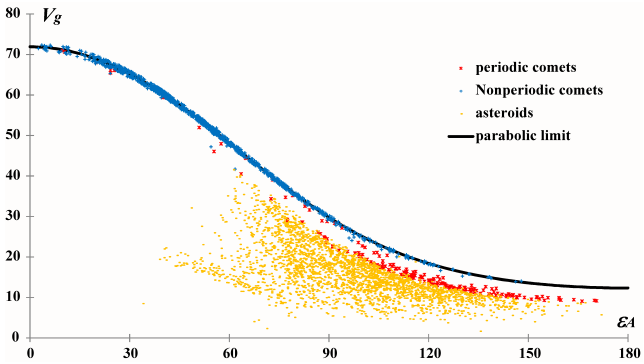

Figure 14 – Geocentric velocity and elongation of radiant from the Apex for the three classes of parent body source.

to it. The number of meteor radiants of non-periodic comets decreases with the elongation from the Apex and those of periodic comets become superior beyond $\varepsilon_A = 90°$. Meteors from asteroids spread over a wider area and have lower geocentric velocity than comets. Figure 14 represents a very suggestive scheme for the studies in section 4.

We know three meteor sources (Apex, ANT and Toroidal) and searched for radiants of three classes of possible parent bodies, but there is no exact correspondence. We here compare the observations with the computed results shown above.

3.2.1 Apex source

The radiant distribution of non-periodic comets (Figure 13b) indicates cometary particles are the origin of the Apex meteors, though it is questionable whether non-periodic comets produce all meteor activities in that area. If non-periodic comets released meteoroids, they would move in very close vicinity to their parent comet and there might be a very rare chance to encounter the Earth.

It seems there is no meteor shower associated with a non-periodic comet and non-periodic comets cannot

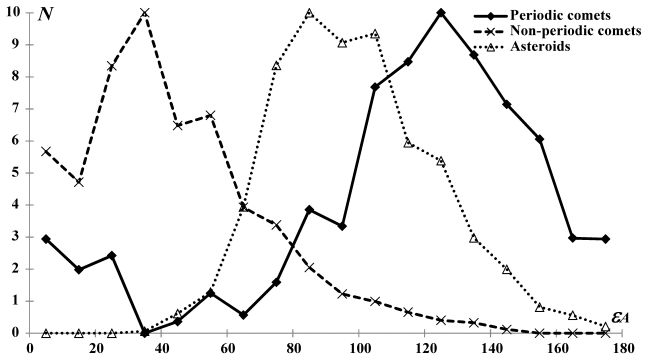

Figure 15 – Density distribution of radiants computed from comets and asteroids, with the elongation from the Apex.

produce meteoroids. But, meteors coming from near the Apex move swiftly as do hypothetical meteors from non-periodic comets. Some of them broke up in our sight, but their debris would not reach us because they moved in close vicinity to their parents and too far from the Earth. A non-periodic comet cannot produce a meteor shower but the offspring of their particles can meet the Earth as sporadic meteors after enough spreading. Non-periodic comets seem to be abundant enough to make a heap of meteors at the Apex source.

Sometimes the Apex source is divided into two parts, north and south. Jones & Brown (1994) suggested the splitting of the Apex source using six surveys catalogued by the IAU Meteor Data Center and ascribed the first report of this phenomenon to Elford & Hawkins (1964). For example, CMOR data suggest the splitting clearly (Campbell-Brown & Wiegert, 2009) but also their figures suggest the splitting of Helion and ANT sources into two parts; north and south. The two branches of the Apex source are not clear in the optical observations (see Figure 23a) and CCD observations indicate rather regional or seasonal activities. North and south Apex might be apparent caused by the geometrical effect and there is no need to discuss their origin separately.

3.2.2 ANT and meteors related to periodic comets

We note the peak of periodic cometary radiants (Figure 15) locates around $\varepsilon_A = 130°$ where meteor activities are scarce (see Figure 7a and 7b). In contrast to cometary radiants, asteroidal radiants' peak coincides with the ANT source (Figure 15). Which is superior in meteor activity, asteroidal meteors or cometary ones? It is noteworthy there is a clear reason why we can see cometary meteors more infrequently.

The maximum (i.e. peak brightness) meteor magnitude $m_{\max}$ changes depending on the pre-atmospheric velocity v_∞. Jacchia et al. (1967) give the following formula. Many researchers have given similar formulae and the coefficient of the second term is between 5 and 10. It is good to use this formula to consider the difference, though this is expressed in cgs:

$$m_{\max} = 55.34 - 8.75 \log v_\infty - 2.25 \log M_\infty - 1.5 \log \cos Z_R$$

Figure 16 compares $m_{\max}$ for different v_∞ as a function of zenith angle Z_R when a pre-atmospheric mass

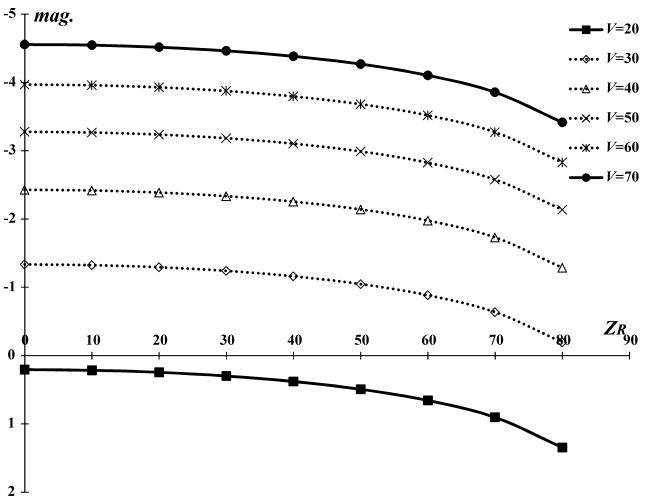

Figure 16 – Comparison of the maximum (peak brightness) meteor magnitude for different pre-atmospheric velocity v_∞ as function of zenith angle Z_R when a pre-atmospheric mass $M_\infty = 1$ g meteoroid enters Earth's atmosphere.

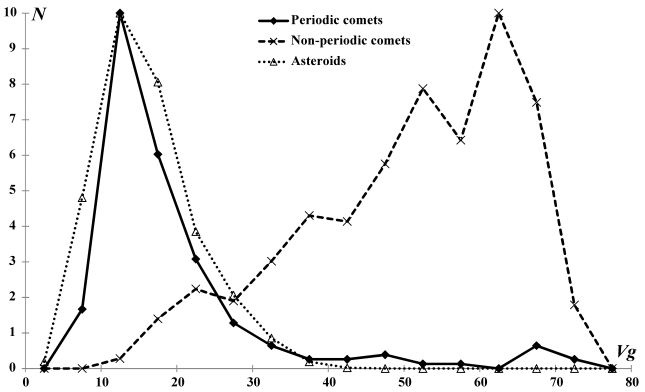

Figure 17 – Distribution of calculated meteors with the geocentric velocity.

$M_\infty = 1$ gram meteoroid enters into the Earth's atmosphere. If we assume M_∞ and Z_R are equal in the above formula, the difference in $m_{\max}$ between $v_\infty = 70$ and $v_\infty = 20$ km/s is 4.76, the gap between the corresponding two lines in Figure 16. This leads us to the result that the ratio of the meteor numbers of the same mass at $v_\infty = 70$ and $v_\infty = 20$ exceeds 100 times, if we apply the magnitude ratio (population index) as $r = 2.63$ and larger. If the Apex meteoroids (represented in Figure 17 around $v_\infty = 70$) and periodic comet particles (slower than $v_\infty = 20$; also in Figure 17) have the same spatial density and the same mass distribution, we see meteors from the former 100 times more than those of the latter.

Differences in magnitude ratios also influence meteor visibilities. We make here the following three assumptions:

1. Observations are limited by meteor magnitude: $m = 2$ might be plausible for the CCD and photo techniques.

2. Meteor groups, though having different magnitude ratios, might have the same meteoroid number at some mass: $M = 1$ g is convenient for

brevity and is used as a preliminary value (see following paragraph).

3. Meteors arrive at the same angle: $Z_R = 90°$ is convenient for brevity.

We can express the meteor number N as a function of meteor magnitude m using the magnitude ratio r as usual:

$$N = N_0\, r^m$$

where N_0 is the meteor number at $m = 0$. We change N_0 so that $N = 1$ at $m = m_{\max}$ by assumption 2; $m_{\max}$ is calculated for $M_\infty = 1$ gram at $Z_R = 90°$ by Jacchia's formula as shown in Figure 16.

We can then obtain cumulative meteor number by integrating the above formula from $-\infty$ to $m = 2$ (assumption 1) normalizing with the new number N_0. Figure 18 shows the differences for various magnitude ratios as a function of v_∞ (V_g for CCD observations). This figure is standardized to a maximum rate of 10 in order to show how the shape of the curve changes for different values of the magnitude ratio r and should not be construed as the difference between N's at the same v_∞. This standardization altered N_0 largely and, therefore, the curves in Figure 18 are moved. If we want to know the real difference between N's for each r, we must survey where the meteoroid number might be the same at $m_{\max}$. It is very difficult to determine such a condition and it is enough for us to study the effect of r on the change of N with v_∞.

Figure 18 shows the more r becomes large, the more the curve becomes steep. It means that a meteoroid group which has larger r could be difficult to recognize at slower v_∞ in contrast with smaller r groups.

We know young meteor showers have greater magnitude ratio than older ones. The magnitude ratio of young Giacobinids is estimated as $r = 3.26$ (Koseki, 1990) and those of older ones are reported elsewhere, Perseids, for example, around $r = 2.0$. We can hardly perceive cometary meteors of fresh particles ejected from comets recently except for a massive enough concentration of meteoroids though we may come across very dispersed ones long after. They will have a smaller magnitude ratio at this later time but become much fewer in spatial density so that we can recognize them as a part of ANT activities, because their orbits would become more circular and their radiants further and further from the Apex. Meteor showers coming from comets are exceptional cases satisfying the following conditions: ejection is massive, meteoroids concentrate within a narrow space, and the collision speed is higher than $V_g = 20$ km/s at least.

3.2.3 Toroidal source

What does 'the Toroidal source' mean? Hawkins, a godfather of meteor science, wrote 'For convenience we call this set of orbits the "toroidal group" because the orbits form a cylindrical toroid in space.' (Hawkins, 1963). There is another and extended usage of 'the Toroidal source': meteors radiate from the Toroidal area, that is, centered at $(\lambda\text{–}\lambda_\odot, \beta)$=(270,65) and 30° in radius.

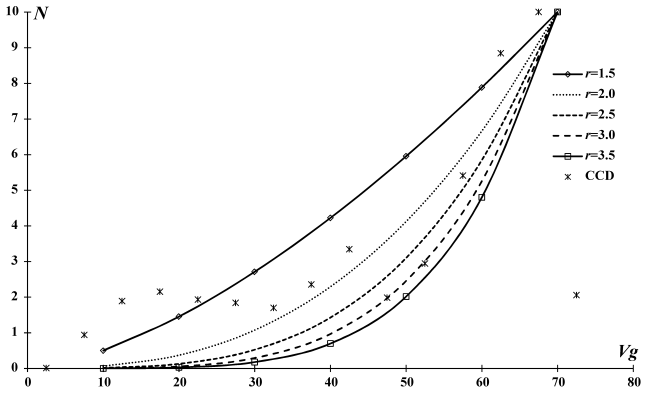

Figure 18 – Change of meteor numbers with velocity for various magnitude ratios r when the meteoroid number equals unity at mass 1 g for each r; maximum rate standardized to 10.

In this extended meaning, 'toroidal meteors' do not construct a 'cylindrical toroid' in every type of observation. Figure 19a represents the distribution of the semi-major axes of radar meteors. As we saw in section 2.1.1, the velocity distribution of radar observations is distorted by its strong selectivity. But there remains the peak around $a = 1$ au after the correction (Taylor & Elford, 1998). Meteors having semi-major axes around $a = 1$ au are the original 'toroidal' ones and this apparent 'toroid' is caused by the nature of Earth based observations.

Optical observations have caught meteors coming from the toroidal area, but such meteors do not always have semi-major axes around $a = 1$ au. Figures 19b–d show the semi-major axis distribution by photo, CCD, and II respectively. Photo and II observations have a smaller peak around $a = 1$ au but there is no indication of such a rise in the CCD distribution. It is clear we can record 'toroidal meteors' by optical techniques but they are mainly of the second meaning, that is, coming from the toroidal region without forming a cylindrical toroid.

We had better consider the toroidal source as having two origins, because optical observations caught meteors orbiting on somewhat larger semi-major axes. We will study this problem in the next section.

4 Where meteoroids are going

The velocity distribution of observed meteors varies with the elongation from the Apex as does that of calculated meteors (see Figure 14). Figure 20a shows the case of photographic meteors as an example. These two figures look alike (three encircled areas correspond to three sources in Figure 14) and suggest meteors have three ancestral sources. It is very interesting that most of the photographic meteors are distributed in the area of 'asteroids'. Are photographic meteors descended from asteroids? Is this caused by velocity bias? We had better compare other observations.

Though every observation type has its preferred favorite velocity, Figures 20b–d confirm the photographic

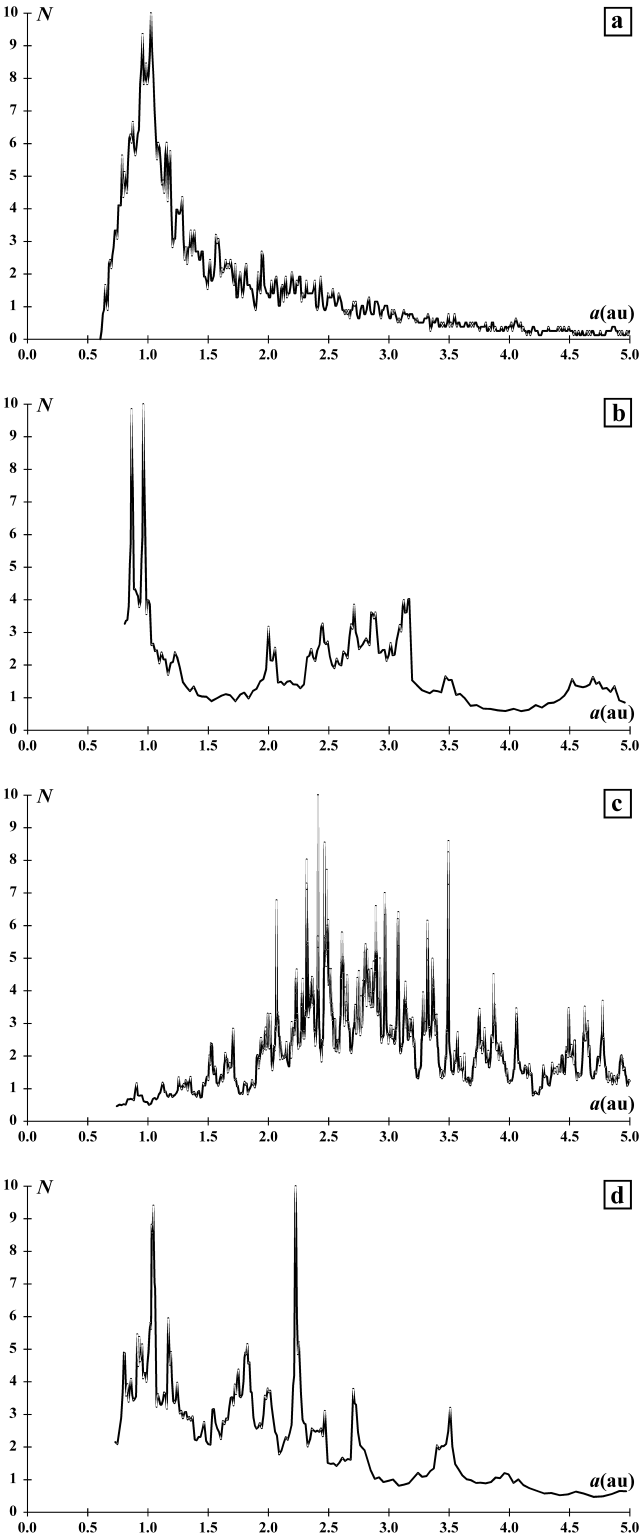

Figure 19 – Semi-major axis distribution of (a) radar; (b) photo; (c) CCD; (d) II meteors.

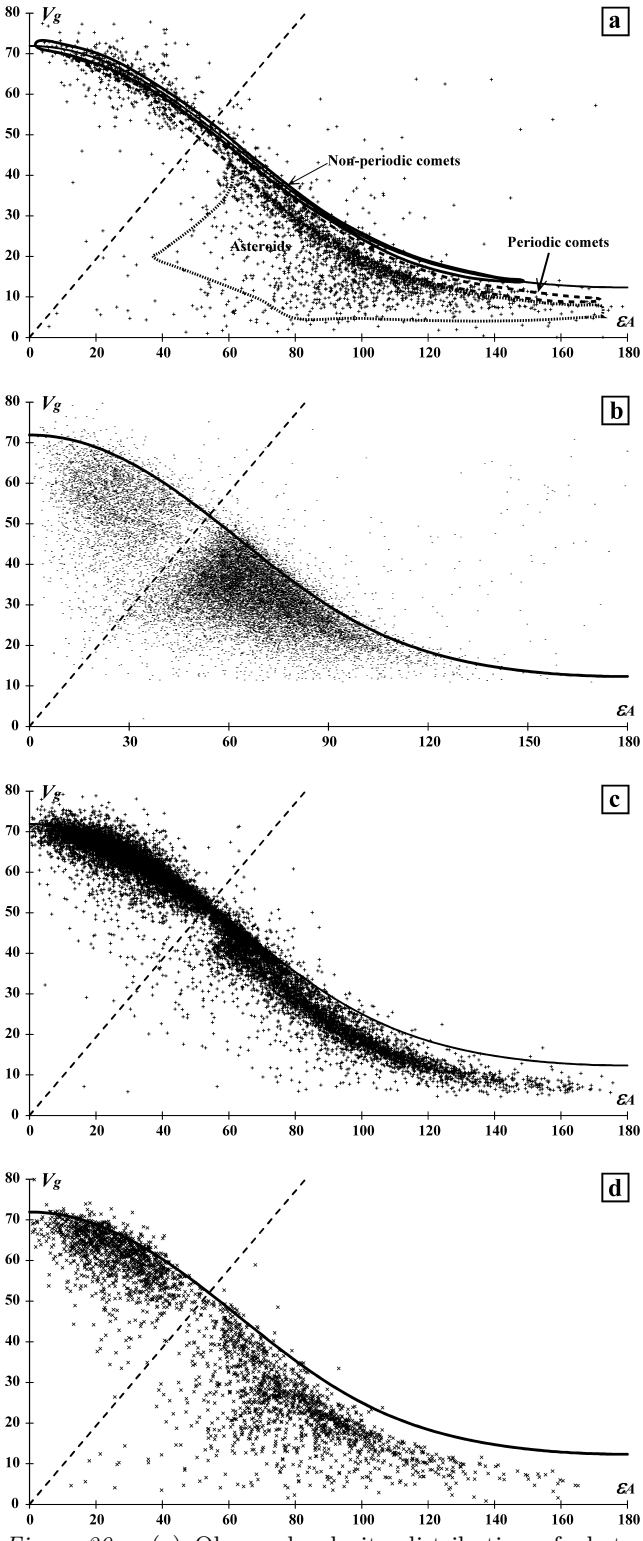

Figure 20 – (a) Observed velocity distribution of photographic meteors with the elongation from the Apex with the calculated radiant areas for comets and asteroids as shown in Figure 14. Dashed line explained in text. (b) radar; (c) CCD; (d) II meteors.

results; many meteors fall in the 'asteroid' area. The most remarkable feature is the discontinuity occurring around $\varepsilon_A = 50°$. We can recognize the gap in radiant distribution surrounding the Apex at 50° radius (see Figure 3a) and confirm it in the corrected velocity distribution (Figure 7b) also. It seems proper to investigate meteors as having two distinct origins, that is, divided by the line through $(\varepsilon_A, V_g) = (54, 52)$ shown in Figures 20a–d as a dashed line. We call the nearer area to the Apex as area **c** (cometary) and the farther as area **a** (asteroidal) hereafter.

4.1 Two distinct sources within the Toroidal region

Why does the radiant gap surrounding the Apex arise? Figure 15 shows the radiants of non-periodic comets ex-

Table 9 – Photographic 'Cyclids' groups found by Koseki (1982).

No.	α	δ	V_g	e	q	i	ω	Ω	$\lambda_\odot$	λ–$\lambda_\odot$	β	N
2	174.0	54.8	3.9	0.128	0.988	5.0	197.5	7.8	7.8	138.6	46.5	7
25	226.8	2.6	3.7	0.117	0.881	2.0	284.8	40.0	40.0	183.6	19.4	12
126	66.4	22.3	3.0	0.108	0.909	0.0	330.8	355.5	355.5	72.8	0.6	21

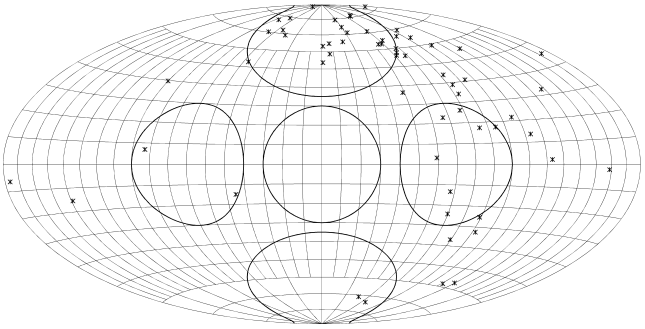

Figure 21 – Radiant distribution of photographic meteors having $e \leq 0.15$ in $(\lambda$–$\lambda_\odot, \beta)$ coordinates.

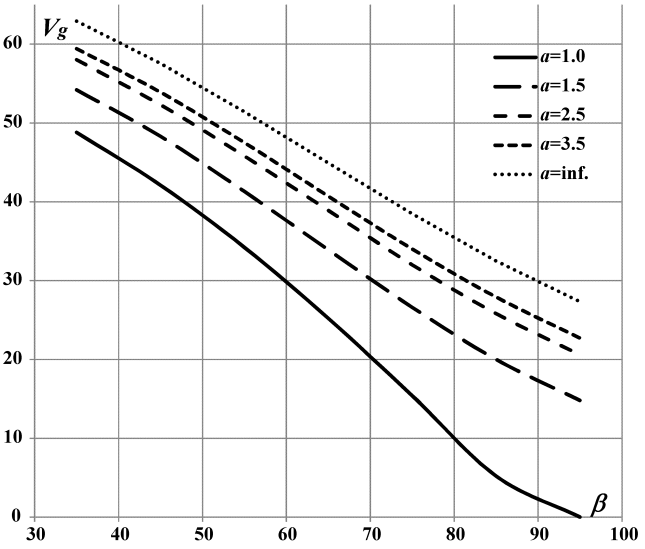

Figure 22 – Geocentric velocity change along longitude line λ–$\lambda_\odot$=270° for meteors having a = 1, 1.5, 2.5 and 3.5 au, and a parabolic orbit. x-axis is β (larger than 90° means over the pole, i.e. λ–$\lambda_\odot$=90° and $\beta' = 180° - \beta$); y-axis is V_g.

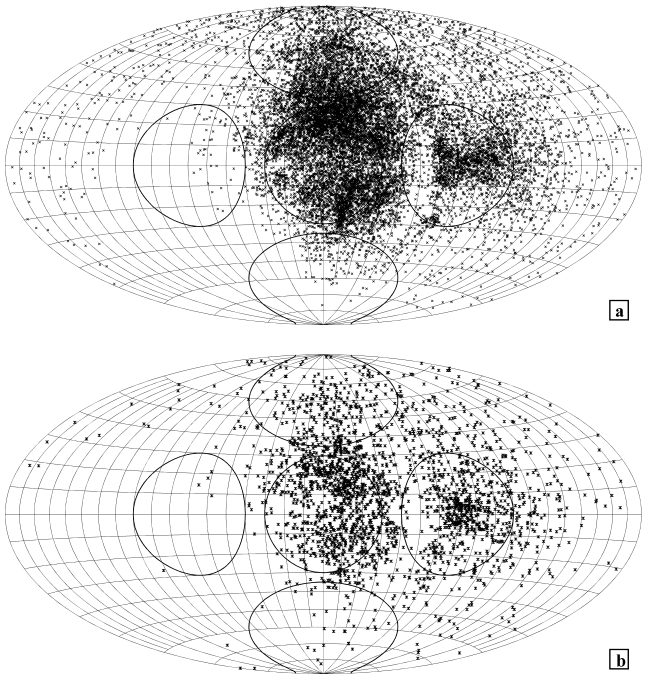

Figure 23 – Radiant distribution in $(\lambda$–$\lambda_\odot, \beta)$ coordinates of (a) CCD; (b) II observations.

ceed those of periodic comets and of asteroids within 50° from the Apex. Figure 17 indicates also meteors faster than V_g = 50 km/s are descended from non-periodic comets. The gap around ε_A = 50° (Figure 3a) corresponds to the dashed line in Figure 20a–d and, therefore, we can realize the area **a** meteors are predominantly associated with non-periodic comets.

Interestingly this gap runs through the Toroidal area. Figures 19b–d show optical observations are different from each other in the distribution of the semi-major axes. It is suggested this difference is caused by the observabilities and by this gap. In photographic meteors, there have been noticed orbits of small eccentricity on low inclined planes, that is, 'Cyclids' (Southworth & Hawkins, 1963). Terenteva (1968) selected 'Cyclids' by the condition: $e \leq 0.14$, aphelion distance $q' \leq 1.2$, $i \leq 15°$. Koseki (1982) detected three groups of Cyclids (Table 9), though they are also of low inclination (ecliptic groups). But, there are several meteors having highly inclined orbits with $e \leq 0.15$ (Figure 21) and some of them seem to be 'toroidal meteors' in the original sense (Hawkins, 1963).

Though CCD observations do not suggest the existence of the cylindrical Toroidal meteors as shown in Figure 19c, the CCD radiant distribution shows the clear concentration in the Toroidal area near to the Apex in contrast with photo. There can be two possibilities: firstly, the difference is caused by their observabilities; alternatively, CCD records the area **c** meteors in the Toroidal area and photo records the area **a** meteors.

Figure 22 shows the geocentric velocity change along the longitude line λ–$\lambda_\odot$=270° for meteors having a = 1 au, a = 1.5 au, a = 2.5 au, a = 3.5 au and parabolic orbits. At β = 35°, the lower border of the Toroidal area, a meteor with V_g = 48.8 km/s comes from an orbit of a = 1 au and V_g = 62.9 km/s from a parabolic orbit. It seems to be very natural that CCD observations are hindered by their favorite velocity (see section 3.1.2) from recording meteors moving with a = 1 au though can catch meteors having elongated orbits. At β = 65°, the center of the Toroidal area, a meteor has V_g = 25.2 km/s if a = 1 au and V_g = 33.9 km/s if a = 1.5 au. It is clear that radar observations draw out the concentration of meteor radiants of 'Toroidal meteors' in the primary meaning. At β = 85° (β = 95° in the

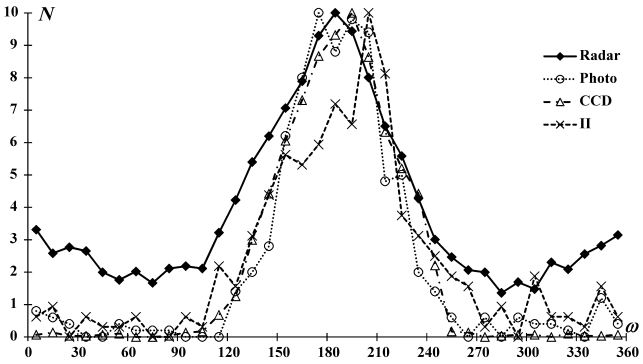

Figure 24 – Argument of perihelion distribution of Toroidal meteors.

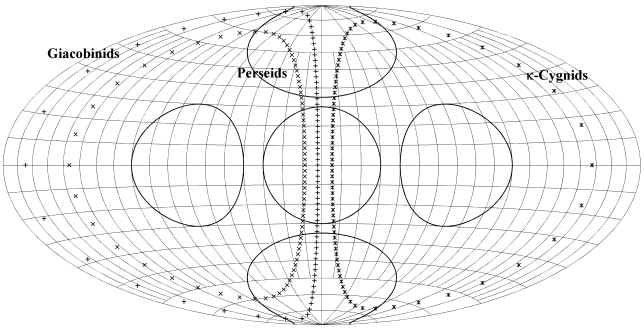

Figure 25 – Radiant shift of analogous showers to Giacobinids (+), Perseids (×) and κ-Cygnids (∗), when we rotate their orbital plane around the node by changing their inclination in 5° intervals.

graph and means λ–$\lambda_\odot$= 90°), the upper (over the pole) border of the Toroidal area, a meteor has V_g = 13.5 km/s, the peak of the photo observability, if a = 1.4 au. Photographic observations easily catch such 'Toroidal' or 'Cyclid' meteors.

It is very interesting that the CCD radiant distribution shows no border between the Apex and the Toroidal and rather makes a heap of radiants between them (see Figure 23a). The distribution of II meteors (Figure 23b) also shows the concentration between them and, moreover, they both suggest the gap between areas **a** and **c** within the 'Toroidal area'. The origin of the Toroidal meteors is not an alternative of non-periodic comets versus asteroids/periodic comets. CCD records more of the Toroidal meteors on the near side to the Apex than the farther side, because the area **c** meteors are nearer to the Apex and faster than those of area **a**. We see both the area **c** meteors and those of area **a** in the 'Toroidal area'.

Figure 24 shows the argument of perihelion of 'Toroidal meteors'. It shows clearly the peaks locate around ω = 180° and this means they encounter the Earth near their perihelion. They hit the Earth at their descending node because we study only north toroidal.

For meteor showers that meet with the Earth near their perihelion, let us consider their orbits rotated around the node, that is, near the fixed perihelion axis of the meteoroid orbit (cf. Condition 1 of Koseki's (2012) hypothesis, given near the start of section 3.1.1 above). We calculate the estimated radiant points altering the inclination in 5° intervals and Figure 25 gives the radiant shift of Giacobinids, Perseids and κ-Cygnids. The results do not mean these three meteor showers would change their orbits in this manner by perturbations but rather that similar types of orbits to these three could bear meteor radiants shown in Figure 25. The Toroidal meteors may come from 'Earth skirting' meteors, the perihelia of which locate near the Earth's orbit.

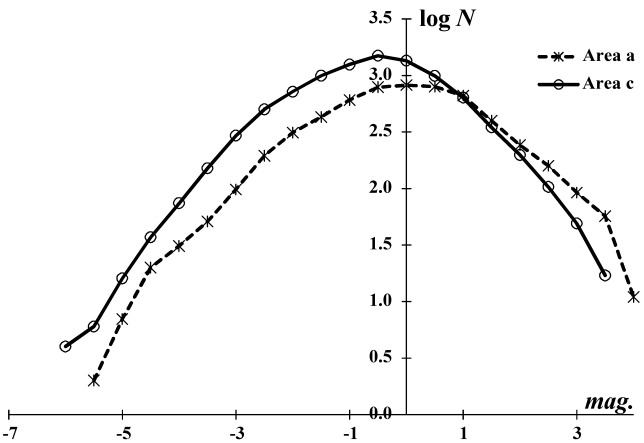

Figure 26 – The magnitude distribution of area **a** and **c** meteors by CCD observations.

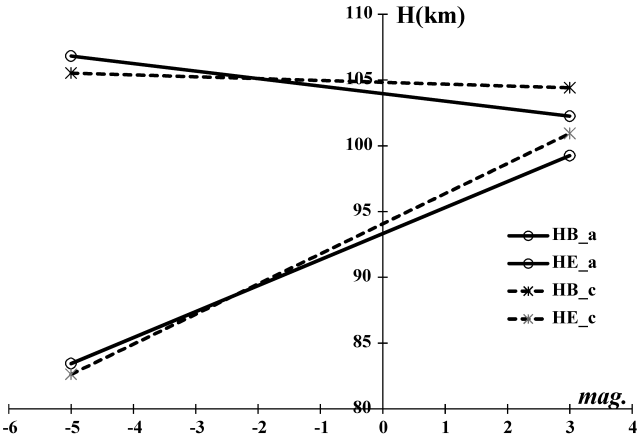

Figure 27 – Comparison of beginning and end height (H_B and H_E) of meteors with V_g between 50 and 60 km/s. The solid line shows the result of the least squares calculation for area **a** and the dashed line for area **c**.

It is noticeable that the distance between neighboring radiants in Figure 25 becomes close in the Toroidal area though the interval of 5° is the same. Geometrical reasons cause this appearance. The concentrations of meteor radiants in the Apex area and in the Toroidal area are strengthened by apparent effects: geometrical position and observability (see section 3.2.2).

When the descendants of Halley type comets or non-periodic comets would become Earth grazing ones, they might be observed as the members of the Toroidal concentration's lower part. When the descendants of asteroid relatives or Jupiter family comets would have perihelion around 1 au, they might be considered as Toroidal meteors, being its upper part. The size of orbits could be altered by the Poynting-Robertson effect and the change in the inclination of orbital planes by perturbations.

4.2 Cometary particles

Is there any difference in physical characteristics of meteoroids between areas **a** and **c**? Firstly, we check the magnitude ratios of meteors in these two areas. Figure 26 gives their magnitude distribution as observed by CCD. It is necessary to use the linear range to get the probable ratio, because they are hindered largely by observabilities in other magnitude ranges. We choose the range from $m = -4.5$ to $m = -2.0$ for area **a** and from $m = -6$ to $m = -2.5$ for area **c**. We get $r = 3.12$ for area **a** and $r = 4.24$ for area **c**. Though the result could be uncertain because of the short range, the magnitude ratio of area **c** might suggest they are of a source rich in smaller particles such as cometary descendants.

Secondly, we compare their beginning and end height (H_B and H_E). We choose meteors between $V_g = 50$ and 60 km/s, because H_B and H_E change with the meteor velocity. Figure 27 shows the summary based on a least squares calculation and area **c** meteors are higher than area **a** meteors in H_E. If we used each study's original definition for the shower classification (see section 2.1), H_B of area **c** meteors would be higher than that of area **a** meteors. This indicates area **c** meteors might be porous and area **a** meteors might penetrate into the lower atmosphere because of their solidity. If the area **a** meteors were borne by comets, their magnitude ratio and physical properties would be same as area **c**. The above results suggest periodic comets do not contribute largely to observed sporadic rates.

Cometary particles released from non-periodic comets will be swept into the Sun by the Poynting-Robertson effect. Wyatt & Whipple (1950) give the following formula:

$$a = \frac{Ce^{\frac{4}{5}}}{1-e^2}\ , \qquad \text{where} \quad C = a_0 e_0^{-\frac{4}{5}}(1-e_0^2)\ .$$

Because a_0 and e_0 are arbitrary values and if we suppose hypothetical particles with $e_0 = 0.99$, $q_0 = 10$ au and $a_0 = 1000$ au, since $q = a(1-e)$, and $e_0 = 0.99$, $q_0 = 5$ au and $a_0 = 500$ au, then we can calculate easily the changes of the eccentricity e with the perihelion distance q shown in Figure 28. It is clear such particles move spirally and pass the Earth's orbit with very low eccentricity; the eccentricity e near the Earth's orbit will be 0.024 in case of $q_0 = 10$ au and $e = 0.061$ for $q_0 = 5$ au. We can observe them as cometary meteors in the Toroidal area and we see the cometary particles in the Apex area if the original perihelion distance is smaller than $q_0 < 1$ au.

4.3 Micro asteroids

On the other hand, does an asteroid bear a meteor shower? There are many suggestive candidates, but it has been unknown how and when the candidates could eject such massive particles as an active comet can. Though not all asteroids produce meteor showers, we can expect many unknown micro asteroids orbiting similarly to detected asteroids. The radiant distribution shown in Figure 13c does not indicate asteroidal meteor showers but can represent sporadic meteor activity by such unknown bodies. There might be many small asteroidal meteoroids which can radiate enough light perceptible by optical observers, though the estimated geocentric velocity is as low as cometary ones (Figure 17). Asteroidal radiants locate far from the Apex (Figures 13c and 15) but near to ANT.

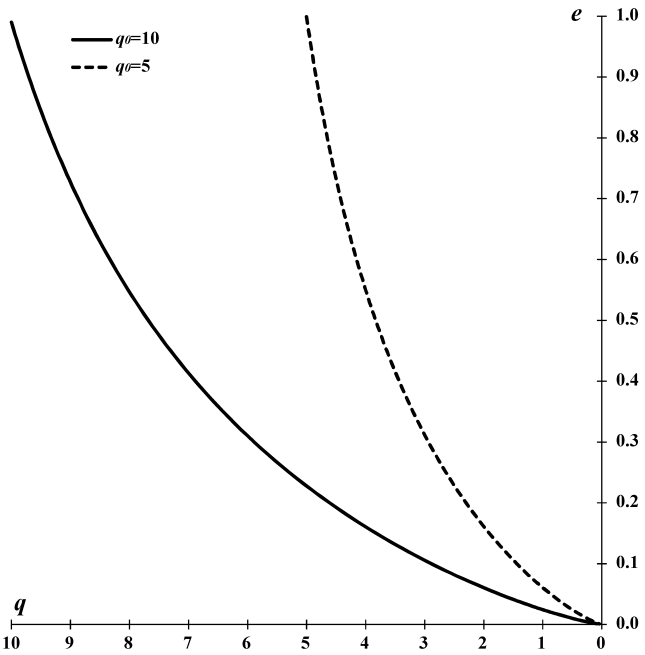

Figure 28 – The changes of the perihelion distance q with the eccentricity e by the Poynting-Robertson effect.

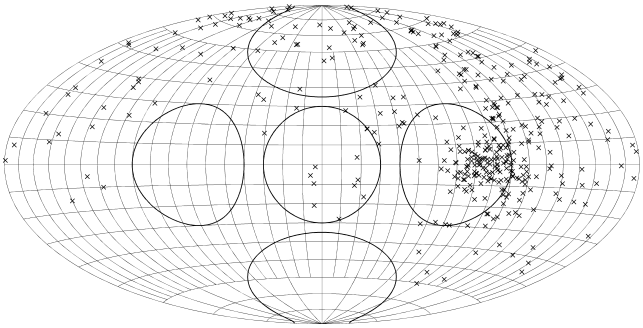

Figure 29 – Radiant distribution in $(\lambda\text{–}\lambda_\odot, \beta)$ coordinates of photo meteors with mass > 1 g. 384 meteors are selected from the IAU database (Neslusan, 2003) excluding those recorded as shower meteors.

Figure 29 shows the radiant distribution of photo meteors heavier than 1 g and this coincides well with the asteroidal radiant distribution (Figure 13c). The ANT center seems to be located at $(\lambda\text{–}\lambda_\odot, \beta)$=(200,0) by visual observations (Figure 2) and radar observations (Figure 3a and 3b). Visual observations include Geminids and Taurids, which shifts the ANT center. Radar observations have a strong bias in velocity as shown in section 3.1.1 and their observability decreases strongly with smaller velocity, that is, with farther elongation from the Apex. The center of radar ANT might be moved apparently by these biases and the real center might coincide with the asteroids' one.

We know meteorites are mainly micro asteroids. Figure 30 gives the radiant distribution of the most pre-

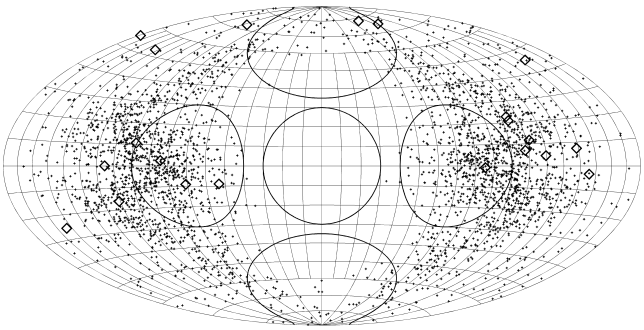

Figure 30 – Radiant distribution in $(\lambda–\lambda_{\odot}, \beta)$ coordinates of the most precisely reduced meteorites (including detected as an asteroid in advance of fall). Meteorite radiants are diamonds and asteroid radiants are small pluses.

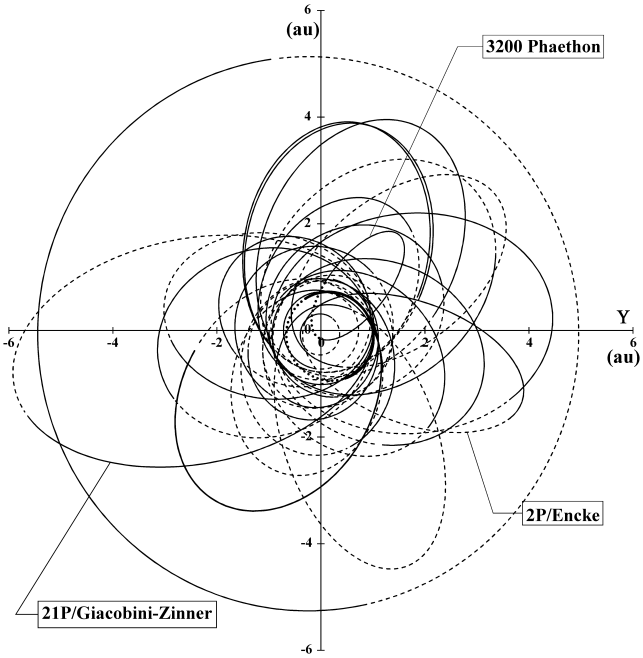

Figure 31 – Orbits of 21 micro asteroids (meteorites) with those of parent comets (or asteroid) of meteor showers. The outmost circle is Jupiter and dashed line indicates the orbit is below the ecliptic plane.

cisely reduced meteorites including those detected as an asteroid in advance of their fall (see Table 10). It is clear the meteorite radiant distribution coincides well with the asteroid one. The meteorite radiant distribution seems to be farther from the Apex than asteroids, because a slower object (a micro asteroid), that is, farther from the Apex, would be more suitable to reach the surface of the Earth and be found as a meteorite.

We know, though, that meteorite falls are witnessed mainly in the evening while the distribution of the asteroid radiants suggests the most plausible time might be in midnight or in broad daylight. Observed numbers of shower meteors reach the maximum when their radiant reaches its highest, but many meteorites fell when their radiants were low on the horizon (see Table 10). This is, however, the corroboration of the asteroidal origin of meteorites, because Sekanina (1983) stressed a meteorite (micro asteroid) would be smashed by the violent increase of air pressure when the zenith distance of its radiant is small, that is, the radiant is high above the horizon.

Figure 31 shows the orbits of 21 micro asteroids (meteorites) with those of some parent comets (or asteroid) of meteor showers. The aphelia of meteorite orbits are located in the main asteroid belt and the shapes of the meteorite orbits look like near-Earth asteroid orbits naturally. It is, therefore, suggested ANT meteors, excluding meteor showers, are descendants mainly from asteroid relatives.

5 Discussion

It is very clear that every observation is affected by a strong dependence of observability on velocity, and we use the observed distribution of the meteor velocity as the observability in this study. But we had better research the reason for such large differences in velocity distribution between optical techniques, though there is a clear difference in radar observations because of its use of the reflection from the ionized column of a meteoroid. Photographic and II meteors have been detected by the human eye on the recorded images but the process is automated in CCD data management. The velocity distributions of photo and of II meteors have bimodal peaks (see Figure 4a) while the number of CCD increases almost monotonically. There are two explanations. Firstly, photo and II are composed of two data sources: Super-Schmidt and so-called small cameras for photographic observations and different focal lenses were used in II observations. It might be suggested that two sources correspond to the two peaks. Secondly, automatic detection of meteors might reject slower meteors by the procedures aiming to avoid false images such as airplanes, bugs etc.

The observability dependence on the velocity is a simple approximation only and it is necessary to study a more plausible one. If we suppose asteroids and comets as parent bodies, the bimodal peaks seem to be natural (see Figure 17). The true velocity distribution should be answered by observations. It is, therefore, necessary to seek the reason for the difference, especially between optical observations as stated above. If bimodal peaks would be confirmed, automated detection of meteors in CCD observations would be better improved to be able to recognize slower meteors excluding disturbances.

If we did not compensate the observability, CCD observations favor the Apex source, radar the Toroidal and II the ANT (see Table 3). It would be natural that radar can catch the faintest meteors and the smallest meteoroids, though the Apex source is the lowest source in radar observations. Correction for the observability by the velocity distribution seems to work well (right part of Table 3) and the order of the different sources' intensities in radar observations becomes: Apex, then Toroidal, then ANT. For optical observations, which record brighter meteors and larger meteoroids, the corrected results reveal a reasonable order: ANT, Toroidal, Apex. The II result shows the Apex source is more intense than the Toroidal one, because II can record fainter meteors than photo and CCD.

Sporadic meteors are neither sons nor daughters of a parent body. Computed meteor activities from comets

and asteroids cannot always show the exact appearance of sporadic meteor displays, though it might be possible to represent the general views. This study shows the first generation meteoroids released from periodic comets may not make the principal contribution to sporadic activities, while meteoroids with asteroidal origins could be important for the ANT source. The radiant distributions of massive (> 1 g) meteors and meteorites support the ANT meteors being the kinsfolk of asteroids.

On the other hand, asteroidal particles cannot play an important role in the Apex activity at all. The only candidate for the Apex source is non-periodic comets and the computed radiant distribution coincides very well with the observations.

Computed radiant distributions differ clearly between non-periodic comets and asteroids and there is a gulf between them. This coincides well with the dip surrounding the Apex source we know of previously. Campbell-Brown (2008) wrote "The source of a ring depleted in meteor radiants at 55° from the apex is attributed to shorter collisional lifetimes inside the ring, due to a higher probability of catastrophic collisions with particles in the zodiacal cloud for the predominantly retrograde meteoroids inside the ring."

The Toroidal source seems to be divided by this 'ring' into two parts; CCD and II record the inner part (the Apex side), radar the central region and photo the outer edge. It might be not necessary to hypothesize 'collisions within the zodiacal cloud'. The Toroidal meteors, not in the primary meaning but secondary, that is, running from that area, are descended from both non-periodic comets and asteroid kinsfolk including periodic comets offspring. Radar observations (Figure 3a) and CCD observations (Figure 23a) reveal bridges connecting the Toroidal source with the ANT (ANT arch) or with the Helion source (Helion arch). These arches might indicate the common origin of ANT and outer part of the Toroidal source, asteroid relatives.

Starting from model particles, Pokorný et al. (2014) concluded "The long-term stable part of the toroidal particles is mainly fed by dust released by Halley type comets" and Jones (2004) indicated "The observed asteroidal meteoroids are predicted to have inclinations close to ±90°". The Toroidal region might be the place of the demise of both origins.

6 Conclusions: answering three questions

We have three questions: 'what meteors are', 'where meteors come from' and 'where meteoroids are going'.

'what meteors are':

A meteor is an atmospheric phenomenon and we cannot see a meteoroid itself. We see a meteor differently with different observational techniques. If we gave no heed to them, we would have a biased view on 'meteors'. We find out the observability of every observational technique depends highly on the meteor velocity. Compensated radiant distributions show: the primary source in radar is the Apex not the Toroidal and in optical observations the ANT.

'where meteors come from':

We looked at the distribution of radiants from where we see meteors coming and compared the radiant points computed from orbits of possible parent bodies of meteors, that is, comets and asteroids. The radiant distribution is divided into two areas; non-periodic comet descendants exceed within the area nearer the Apex $\varepsilon_A < 60°$ and asteroid kinsfolk predominate over the remaining greater part.

'where meteoroids are going':

Many average meteors we see are older than the Giacobinids or other such young meteors. Sporadic meteors had originated tens of thousands of years ago and were carried to their present place by some forces. We can study these changes in meteoroid orbits and learn their future. Particles related to non-periodic comets would be affected by the Poynting-Robertson effect and their orbits become near circular when they would approach the Earth's orbit. NEOs (Near Earth Objects) have a mainly asteroidal nature and moved from the main asteroid belt into the present orbit by perturbations or by collisions. We meet both of them on their way to the Sun.

References

Beatty K. (2014). "Small asteroid 2014 AA hits Earth". http://www.skyandtelescope.com/astronomy-news/small-asteroid-2014-aa-hitsearth/ .

Beech M., Brown P., Hawkes R. L., Ceplecha Z., Mossman K., and Wetherill G. (1995). "The fall of the Peekskill meteorite: Video observations, atmospheric path, fragmentation record and orbit". *Earth, Moon, and Planets*, **68**, 189–197. Videos: http://meteor.uwo.ca/~pbrown/Videos/peekskill.htm and http://fireball.meteorite.free.fr/meteor/en/1/1992-10-09/peekskill/synthese.

Borovička J., Spurný P., Kalenda P., and Tagliaferri E. (2003). "The Morávka meteorite fall: 1. Description of the events and determination of the fireball trajectory and orbit from video records". *Meteorit. Planet. Sci.*, **38**, 975–987.

Borovička J., Tóth J., Igaz A., Spurný P., Kalenda P., Haloda J., Svoreň J., Kornoš L., Silber E., Brown P., and Husárik M. (2013). "The Košice meteorite fall: Atmospheric trajectory, fragmentation, and orbit". *Meteorit. Planet. Sci.*, **48**, 1757–1779.

Brown P., McCausland P. J. A., Fries M., Silber E., Edwards W. N., Wong D. K., Weryk R. J., Fries J., and Krzeminski Z. (2011). "The fall of the Grimsby meteorite—I: Fireball dynamics and orbit from radar, video, and infrasound records". *Meteorit. Planet. Sci.*, **46**, 339–363.

Brown P., Pack D., Edwards W. N., ReVelle D. O., Yoo B. B., Spalding R. E., and Tagliaferri E. (2004).

"The orbit, atmospheric dynamics, and initial mass of the Park Forest meteorite". *Meteorit. Planet. Sci.*, **39**, 1781–1796.

Brown P. G. et al. (2000). "The fall, recovery, orbit, and composition of the Tagish Lake meteorite: A new type of carbonaceous chondrite". *Science*, **290**, 320–325.

Campbell-Brown M. D. (2008). "High resolution radiant distribution and orbits of sporadic radar meteoroids". *Icarus*, **196**, 144–163.

Campbell-Brown M. D. and Wiegert P. (2009). "Seasonal variations in the north toroidal sporadic meteor source". *Meteorit. Planet. Sci.*, **44**, 1837–1848.

Ceplecha Z., Rajchl J., and Sehnal L. (1959). "New Czechoslovak meteorite "Luhy"". *Bull. Astron. Inst. Czechoslov.*, **10**, 147–148.

Elford W. G. and Hawkins G. S. (1964). "Meteor echo rates and the flux of sporadic meteors". Harvard Radio Meteor Project Research Report No. 9.

Haack H., Grau T., Bischoff A., Horstmann M., Wasson J., Sørensen A., Laubenstein M., Ott U., Palme H., Gellissen M., Greenwood R. C., Pearson V. K., Franchi I. A., Gabelica Z., and Schmitt-Kopplin P. (2012). "Maribo—A new CM fall from Denmark". *Meteorit. Planet. Sci.*, **47**, 30–50.

Halliday I., Blackwell A. T., and Griffin A. A. (1978). "The Innisfree meteorite and the Canadian camera network". *J. Roy. Astron. Soc. Can.*, **72**, 15–39.

Hawkins G. S. (1963). "The Harvard Radio Meteor Project". *Smithson. Contrib. Astrophys.*, **7**, 53–62.

IAUMDC (2015). "Meteor data center". `http://www.astro.amu.edu.pl/~jopek/MDC2007/` . (Updated 2015 June 22, by Z. Kanuchova and T. J. Jopek).

Jacchia L. G., Verniani F., and Briggs R. E. (1967). "An analysis of the atmospheric trajectories of 413 precisely reduced photographic meteors". *Smithson. Contrib. Astrophys.*, **10**, 1–139.

Jenniskens P. et al. (2012). "Radar-enabled recovery of the Sutter's Mill meteorite, a carbonaceous chondrite regolith breccia". *Science*, **338**, 1583–1587.

Jenniskens P. et al. (2014). "Fall, recovery and characterization of the Novato L6 chondrite breccia". *Meteorit. Planet. Sci.*, **49**, 1388–1425. See also: `http://cams.seti.org/index-N.html`.

Jenniskens P., Vaubaillon J., Binzel R. P., DeMeo F. E., Nesvorný D., Bottke W. F., Fitzsimmons A., Hiroi T., Marchis F., Bishop J. L., Vernazza P., Zolensky M. E., Herrin J. S., Welten K. C., Meier M. M. M., and Shaddad M. H. (2010). "Almahata Sitta (= asteroid 2008 TC_3) and the search for the ureilite parent body". *Meteorit. Planet. Sci.*, **45**, 1590–1617.

Jones J. (2004). "Meteoroid engineering model – final report". SEE/CR-2004-400. NASA.

Jones J. and Brown P. (1994). "The radiant distribution of sporadic meteors". *Planet. Space Sci.*, **42**, 123–126.

JPL (2015). "Small-body database browser". `http://ssd.jpl.nasa.gov/sbdb.cgi` .

Kasheev B. L., Lebedinets V. N., and Lagutin M. F. (1967). *Meteoric Phenomena in the Earth's Atmosphere. (Investigations meteor No. 2)*. Nauka. Page 84. (In Russian).

Koseki M. (1982). "Meteor shower research on photographic meteors by cluster analysis". *23rd Japanese Meteor Conference*. (In Japanese).

Koseki M. (1990). "Observations of the 1985 Giacobinids in Japan". *Icarus*, **88**, 122–128.

Koseki M. (2009). "Meteor shower records: A reference table of observations from previous centuries". *WGN, Journal of the IMO*, **37:5**, 139–160.

Koseki M. (2012). "A simple model of spatial structure of meteoroid streams". *WGN, Journal of the IMO*, **40:5**, 162–165.

Koseki M. (2014). "Various meteor scenes I: The perception and the conception of a 'meteor shower'". *WGN, Journal of the IMO*, **42:5**, 170–180.

Lindblad B. A. and Steel D. I. (1994). "Meteoroid orbits available from the IAU Meteor Data Center". In Milani A., Di Martino M., and Cellino A., editors, *Asteroids, Comets, Meteors 1993, IAU Symp. No. 160*. Kluwer, pages 497–501. Also: `http://sbn.psi.edu/pds/asteroid/EAR_A_VARGBDET_5_METORB_V1_0/data/`.

McCrosky R. E., Posen A., Schwartz G., and Shao C.-Y. (1971). "Lost City meteorite – its recovery and a comparison with other fireballs". SAO Special Report No. 336.

McKinley D. W. R. (1961). *Meteor Science and Engineering*. McGraw-Hill. Page 56.

Milley E. P., Hildebrand A. R., Brown P. G., Noble M., Sarty G., Ling A., and Maillet L. A. (2010). "Pre-fall orbit of the Buzzard Coulee meteoroid". AAPG Search & Discovery Article #90172, CSPG/CSEG/CWLS GeoConvention, Calgary, May 10–14, 2010.

Neslusan L. (2003). "IAU Meteor Data Center Photographic Database". `http://www.astro.sk/~ne/IAUMDC/Ph2003/database.html` .

Olivier C. P. (1960). "Catalog of hourly meteor rates". *Smithson. Contrib. Astrophys.*, **4**, 1–14.

Pokorný P., Vokrouhlický D., Nesvorný D., Campbell-Brown M., and Brown P. (2014). "Dynamical model for the toroidal sporadic meteors". *Astrophys. J.*, **789**, 25 (20pp).

Popova O. P. et al. (2013). "Chelyabinsk airburst, damage assessment, meteorite recovery, and characterization". *Science*, **342**, 1069–1073. Videos: `http://newswatch.nationalgeographic.com/2013/02/15/best-videos-from-meteor-strike-in-russia/`.

Sekanina Z. (1983). "The Tunguska event: No cometary signature in evidence". *Astron. J.*, **88**, 1382–1413.

Shanklin J. (2015). "SOHO and STEREO comets". `http://www.ast.cam.ac.uk/~jds/klist.htm` . BAA & SPA Comet Section.

Shigeno Y. and Yamamoto M.-Y. (2012). "Meteor shower catalog based on 3770 triangulation analyses of double-station image-intensified video observations over Japan". *WGN, Journal of the IMO*, **40:1**, 24–35. Also: `http://www.imo.net/files/data/msswg/msswg.txt`.

SonotaCo (2014). "SonotaCo Network simultaneously observed meteor data sets". `http://sonotaco.jp/doc/SNM/` .

Southworth R. B. and Hawkins G. S. (1963). "Statistics of meteor streams". *Smithson. Contrib. Astrophys.*, **7**, 261–285.

Spurný P., Bland P. A., Shrbený L., Borovička J., Ceplecha Z., Singelton A., Bevan A. W. R., Vaughan D., Towner M. C., McClafferty T. P., Toumi R., and Deacon G. (2012). "The Bunburra Rockhole meteorite fall in SW Australia: fireball trajectory, luminosity, dynamics, orbit, and impact position from photographic and photoelectric records". *Meteorit. Planet. Sci.*, **47**, 163–185.

Spurný P., Bland P. A., Shrbený L., Towner M. C., Borovička J., Bevan A. W. R., and Vaughan D. (2011). "The Mason Gully meteorite fall in SW Australia: Fireball trajectory and orbit from photographic records". 74th Annual Meteoritical Society Meeting, paper 5101.

Spurný P., Borovička J., Kac J., Kalenda P., Atanackov J., Kladnik G., Heinlein D., and Grau T. (2010). "Analysis of instrumental observations of the Jesenice meteorite fall on April 9, 2009". *Meteorit. Planet. Sci.*, **45**, 1392–1407.

Spurny P., Heinlein D., and Oberst J. (2002). "The atmospheric trajectory and heliocentric orbit of the Neuschwanstein meteorite fall on April 6, 2002". In Warmbein B., editor, *Proc. Asteroids, Comets, Meteors 2002 Berlin, ESA SP-500*. ESA, Noordwijk, pages 137–140.

Taylor A. D. and Elford W. G. (1998). "Meteoroid orbital element distributions at 1 AU deduced from the Harvard Radio Meteor Project observations". *Earth Planets Space*, **50**, 569–575.

Terenteva A. K. (1968). "Investigation of minor meteor streams". In Kresák L. and Millman P. M., editors, *Physics and Dynamics of Meteors, IAU Symp. No. 33*. D. Reidel, pages 408–427.

Trigo-Rodríguez J. M., Borovička J., Spurný P., Ortiz J. L., Docobo J. A., Castro-Tirado A. J., and Llorca J. (2006). "The Villalbeto de la Peña meteorite fall: II. Determination of atmospheric trajectory and orbit". *Meteorit. Planet. Sci.*, **41**, 505–517.

Wyatt S. P. and Whipple F. L. (1950). "The Poynting-Robertson effect on meteor orbits". *Astrophys. J.*, **111**, 134–141.

Handling Editor: David Asher

Table 10 – 20 precisely reduced meteorites and one candidate meteorite fallen in the Atlantic ocean. References: (1) (Ceplecha et al., 1959) [Orbital data from (Spurny et al., 2002)]. (2) (McCrosky et al., 1971). (3) (Halliday et al., 1978). (4) (Beech et al., 1995). (5) (Brown et al., 2000). (6) (Borovička et al., 2003). (7) (Spurny et al., 2002). (8) (Brown et al., 2004). (9) (Trigo-Rodríguez et al., 2006). (10) (Spurný et al., 2012). (11) (Jenniskens et al., 2010). (12) (Milley et al., 2010). (13) (Haack et al., 2012). (14) (Spurný et al., 2010). (15) (Brown et al., 2011). (16) (Borovička et al., 2013). (17) (Spurný et al., 2011). (18) (Jenniskens et al., 2012). (19) (Jenniskens et al., 2014). (20) (Popova et al., 2013). (21) (Beatty, 2014).

Name	Place	Year	Month	Day	Time (LT)	α	δ	V_g	a	e	q	i	ω (peri)	Ω (node)	Type	Ref.
Příbram	Czechoslov.	1959	4	7	$20^h30^m20^s$	192.343	+17.461	17.427	2.401	0.6711	0.78951	10.478	241.738	17.80285	H5	(1),
						±0.011	±0.002	±0.006	±0.002	±0.0003	±0.00006	±0.004	±0.015	±0.00001		(7)
Lost City	USA	1970	1	4	20^h14^m	315.5	+39.3	8.8	1.66	0.417	0.967	12.00204	160.9702	283.7277	H5	(2)
Innisfree	Canada	1977	2	5	$19^h17^m38^s$	7.4	+66.5	14.54	1.872	0.4732	0.986	12.27514	177.9511	317.517	L5	(3)
Peekskill	USA	1992	10	9	19^h50^m	209.6	−29.3	10.1	1.49	0.41	0.886	4.9	308	17.030	H6	(4)
									±0.03	±0.01	±0.004	±0.2	±1	±0.001		
Tagish Lake	Canada	2000	1	18	$08^h43^m42^s$	88.0	+27.9	11.3	2.1	0.57	0.891	1.4	222	297.900	C2-ung	(5)
									±0.2	±0.05	±0.009	±0.9	±2	±0.003		
Morávka	Czech Republic	2000	5	6	$12^h51^m52^s$	250.1	+54.96	19.6	1.85	0.47	0.9823	32.2	203.5	46.2580	H5	(6)
						±0.7	±0.24	±0.4	±0.07	±0.02	±0.0009	±0.5	±0.6			
Neuschwanstein	Germany	2002	4	6	$21^h20^m17^s.7$	192.33	+19.58	17.51	2.4	0.670	0.7931	11.43	241.1	16.82666	EL6	(7)
						±0.09	±0.13	±0.05	±0.02	±0.003	±0.0009	±0.06	±0.2	±0.00001		
Park Forest	USA	2003	3	26	23^h50^m	171.8	+11.2	16.1	2.53	0.680	0.811	3.2	237.5	6.1156	L5	(8)
						±1.3	±0.5	±0.4	±0.19	±0.023	±0.008	±0.3	±1.6	±0.0007		
Villalbeto de la Peña	Spain	2004	2	4	$17^h46^m45^s.2$	311.4	−18.0	16.9	2.3	0.63	0.860	0.0	132.3	283.6712	L6	(9)
						±1.3	±0.7	±0.4	±0.2	±0.04	±0.007	±0.2	±1.5			
Bunburra Rockhole	Australia	2007	7	21	$04^h43^m57^s$	80.73	+14.21	6.743	0.8529	0.2427	0.6459	8.95	210.04	297.595	Eucrite	(10)
						±0.06	±0.04	±0.014	±0.0004	±0.0005	±0.0007	±0.03	±0.06			
Almahata Sitta	Sudan	2008	10	7	05^h46^m	348.5	+7.7	7.1	1.308201	0.312065	0.899957	2.5422	234.449	194.1011	Ureilite-an	(11)
Buzzard Coulee	Canada	2008	11	20	$17^h26^m45^s$	285.3	+77.3	14.3	1.225	0.215	0.961	25.486	212.019	238.937	H4	(12)
Maribo	Denmark	2009	1	17	$20^h08^m28^s$	124.6	+18.8	25.4	2.34	0.795	0.481	0.72	99.0	117.64	CM2	(13),
						±1.0	±1.6	±0.8	±0.29	±0.026	±0.010	±0.98	±1.4	±0.05		(18)
Jesenice	Slovenia	2009	4	9	$02^h59^m40^s.5$	159.9	+58.7	8.3	1.75	0.431	0.9965	9.6	190.5	19.196	L6	(14)
						±1.2	±0.5	±0.4	±0.07	±0.022	±0.0006	±0.5	±0.5			
Grimsby	Canada	2009	9	25	21^h03^m	242.61	+54.97	17.89	2.04	0.518	0.9817	28.07	159.865	182.9561	H5	(15)
						±0.26	±0.12	±0.22	±0.05	±0.011	±0.0004	±0.28	±0.43			
Košice	Slovakia	2010	2	28	$22^h24^m46^s$	114.3	+29.0	10.3	2.71	0.647	0.957	2.0	204.2	340.072	H5	(16)
						±1.7	±3.0	±0.5	±0.24	±0.032	±0.004	±0.8	±1.2	±0.004		
Mason Gully	Australia	2010	4	13	$18^h36^m10^s$	148.4	+9.2	9.2	2.470	0.6023	0.98240	0.832	18.95	203.2112	H5	(17)
									±0.004	±0.0007	±0.00007	±0.013	±0.03			
Sutter's Mill	USA	2012	4	22	$07^h51^m12^s$	24.0	+12.7	26.0	2.59	0.824	0.456	2.38	77.8	32.77	C	(18)
						±1.3	±1.7	±0.7	±0.35	±0.020	±0.022	±1.16	±3.2	±0.06		
Novato	USA	2012	10	17	$19^h44^m29^s.88$	268.1	−48.9	8.21	2.09	0.526	0.9880	5.5	347.37	24.9414	L6	(19)
						±0.6	±0.7	±0.22	±0.11	±0.024	±0.0003	±0.6	±0.18	±0.0005		
Chelyabinsk	Russia	2013	2	15	$09^h20^m32^s.2$	333.2	+0.3	15.3	1.76	0.581	0.739	4.93	108.3	326.4422	LL5	(20)
						±1.6	±1.8	±0.4	±0.16	±0.018	±0.020	±0.48	±3.8	±0.0028		
2014 AA	Atlantic	2014	1	2	00^h	82.4	+14.3	5.1	1.164276	0.213168	0.91609	1.425552	52.28165	101.5794		(21)

Four possible new high-declination showers

Damir Šegon[1], *Peter Gural*[2], *Željko Andreić*[3], *Denis Vida*[4], *Ivica Skokić*[5], *and Filip Novoselnik*[6]

Four possible new meteor showers described in this paper are last ones resulting from our search for new meteor showers. All four of them seem to be connected to known parent bodies, currently classified as asteroids. All orbits from which associations had been done are orbits calculated by UFOOrbit software. Mean orbital parameters were computed using simple arithmetic average in an iterative way until stable set of orbits was found. Catalogues from 2007 to 2011 (SonotaCo) and 2007 to 2010 (CMN) were used in calculations. The radiants' dispersion is in all cases large and no clear radiant drift may be seen, possibly due to the fact that meteoroid streams from these parent bodies suffer from significant perturbations and we see these showers at different solar longitudes from year to year.

Received 2015 August 31

1 Introduction

New showers found as the result of Croatian Meteor Network shower search (Šegon et al., 2014b) in SonotaCo (SonotaCo, 2009; SonotaCo, 2005–2013) and CMN (Šegon et al., 2012; Korlević et al., 2013) orbit databases (in total 133 652 orbits) were published in *WGN* since 2013. In this paper we present the most recent 4 ones resulting from our search, all of them possibly associated with parent bodies at the moment considered as asteroids. Mean orbital parameters were computed as described in (Šegon et al., 2014a), using a simple arithmetic average on the dataset in iterative way until stabile set of orbits has been found. Orbital data used ranges from 2007 to 2011 (SonotaCo) and 2010 (CMN), leaving space for further investigation of these possible new showers in other databases available at the present. As before, for orbital similarity a multiple D-criterion was used. In this procedure, the following three D-criteria are used: (D_{SH} (Southworth & Hawkins, 1963), D_{D} (Drummond, 1981) and D_{H} (Jopek, 1993)). All three have to be satisfied simultaneously, as follows: $D_{\mathrm{SH}} \leq 0.15$, $D_{\mathrm{H}} \leq 0.15$ and $D_{\mathrm{D}} \leq 0.075$.

The most important facts about 4 showers described in this article are summarized in the Table 5.

[1]Astronomical Society Istra Pula, Park Monte Zaro 2, 52100 Pula, Croatia. Višnjan Science and Education Center, Istarska 5, 51463 Višnjan, Croatia. Email: damir.segon@pu.htnet.hr

[2]351 Samantha Drive, Sterling, VA 20164-5539, USA. Email: peter.s.gural@saic.com

[3]University of Zagreb, Faculty of Mining, Geology and Petroleum Engineering, Pierottijeva 6, 10000 Zagreb, Croatia. Email: zandreic@rgn.hr

[4]Astronomical Society "Anonymus", B. Radića 34, 31550 Valpovo, Croatia and Faculty of Electrical Engineering, University of Osijek, Kneza Trpimira 2B, 31000 Osijek, Croatia. Email: denis.vida@gmail.com

[5]Astronomical Society "Anonymus", B. Radića 34, 31550 Valpovo, Croatia. Email: ivica.skokic@gmail.com

[6]Astronomical Society "Anonymus", B. Radića 34, 31550 Valpovo, Croatia and Faculty of Electrical Engineering, University of Osijek, Kneza Trpimira 2B, 31000 Osijek, Croatia. Email: filip.novoselnik@gmail.com

IMO bibcode WGN-435-segon-highdec
NASA-ADS bibcode 2015JIMO...43..147S

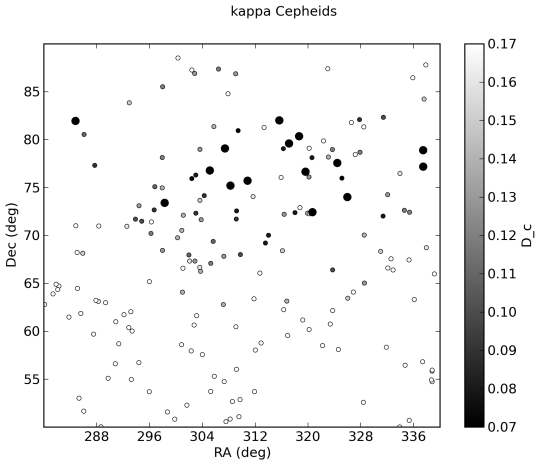

Figure 1 – The radiant plot of the κ Cepheids.

2 κ Cepheids

The κ Cepheids shower (Figure 1) is active from September 11 to September 23 with the maximum falling roughly on September 17. Individual radiants of meteors belonging to this shower are scattered over a relatively large area of the sky. The daily motion in RA turned out to be negative, a fact that we see often in connection with showers with possible asteroidal origin (Šegon et al., 2014). The activity seems to be more or less constant over most of the activity period. 17 individual meteor orbits were found by our search. The individual orbits are very compact, with average D_{SH} to the mean orbit of only 0.06, and the maximal D_{SH} found is 0.08. There are no known showers in the vicinity.

Table 1 – Comparison of orbital elements of κ Cepheids (mean orbit) and the orbit of asteroid 2009 SG18.

parameter	751 KCE	2009 SG18
q	0.983	0.993
e	0.664	0.672
ω	198.4	204.1
Ω	174.4	177.6
i	57.7	58.4
D_{SH}	0.100	
D_{H}	0.100	
D_{D}	0.034	

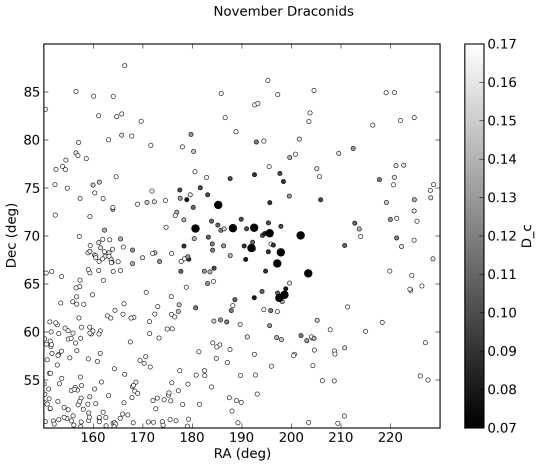

Figure 2 – The radiant plot of the November Draconids.

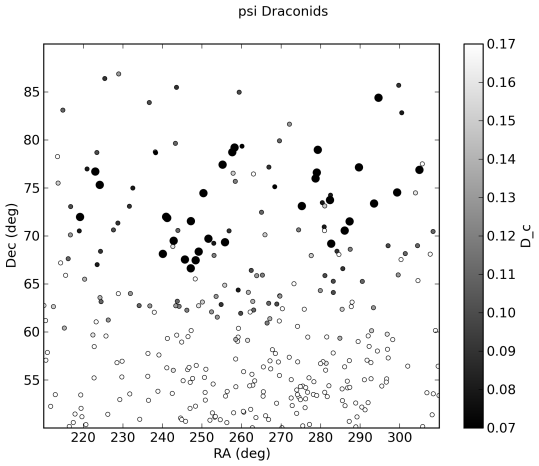

Figure 3 – The radiant plot of the ψ Draconids.

Additionally, the mean orbit of the shover is similar to the orbit of asteroid 2009 SG18 (see Table 1, indicating possible connection between them).

3 November Draconids

The November Draconids shower (Figure 2) is active from November 8 to November 20 with the maximum falling roughly on November 16. The radiant plot shows spread of individual meteor radiants due to the daily motion, but is otherwise compact. The activity seems to be more or less constant over most of the activity period. 12 individual meteor orbits were found by our search. Again, the individual orbits are very compact, with average D_{SH} to the mean orbit of only 0.06, and the maximal D_{SH} found is 0.08.

Nearby is one already known shower, the December alpha Draconids (334 DAD), for which IAU MDC database (Jopek & Kaňuchová, 2014) does not quote any orbital elements. We have, however, detected this shower too in our search, and were able to calculate its mean orbital elements. The comparison between mean orbits of 753 NED and 334 DAD is given in the Table 2.

Last, but not least, the mean orbit of this shower is similar to the orbit of asteroid 2009 WN25 (see Table 2), indicating possible connection between them.

Table 2 – Comparison of orbital elements of November Draconids (mean orbit), December alpha Draconids and asteroid 2009 WN25. Orbital element sets for both showers were determined from our data.

parameter	753 NED	334 DAD	2009 WN25
q	0.987	0.983	1.102
e	0.701	0.590	0.661
ω	183.7	178.2	180.9
Ω	232.8	254.1	232.1
i	73.5	72.7	72.0
D_{SH}		0.370	0.130
D_{H}		0.370	0.082
D_{D}		0.158	0.064

4 ψ Draconids

The ψ Draconids shower (Figure 3) is active from March 19 to April 12 with the maximum falling roughly on April 2. The radiant plot shows the spread of individual meteor radiants due to the daily motion, and is very diffuse. The activity seems to be more or less constant over most of the activity period. 31 individual meteor orbits were found by our search. As is the case with previously described showers, the individual orbits are very compact, with average D_{SH} to the mean orbit of only 0.06, and the maximal D_{SH} found is 0.08.

The phi Draconids (045 PDF) shower is nearby. Again, we calculated its mean orbital elements from our data (see Table 3). These two showers are clearly different, but could be related to each other. This will be further investigated in a forthcoming publication.

Last, but not least, the mean orbit of this shover is similar to the orbit of asteroid 2008 GV (see Table 3), indicating possible connection between them.

5 May ι Draconids

The May ι Draconids shower (Figure 4) is active from May 7 to June 6 with the maximum falling roughly on May 21. The radiant plot is very diffuse and does not show clear effects of daily motion. Calculations confirm this, showing very small daily motion in RA. The activity seems to be more or less constant over most of the activity period. 19 individual meteor orbits were found by our search. Again, the individual orbits are

Table 3 – Comparison of orbital elements of ψ Draconids (mean orbit), ϕ Draconids and asteroid 2008 GV.

parameter	754 POD	045 PDF	2008 GV
q	0.994	0.990	1.067
e	0.622	0.613	0.609
ω	179.3	184.4	177.6
Ω	11.8	353.0	15.6
i	30.9	39.4	30.1
D_{SH}		0.263	0.084
D_{H}		0.263	0.055
D_{D}		0.092	0.040

Table 4 – Comparison of orbital elements of May ι Draconids (mean orbit) and asteroid 2006 GY2.

parameter	755 MID	2006 GY2
q	0.989	0.936
e	0.604	0.496
ω	198.1	216.7
Ω	60.2	54.3
i	24.3	30.6
D_{SH}	0.212	
D_{H}	0.208	
D_{D}	0.117	

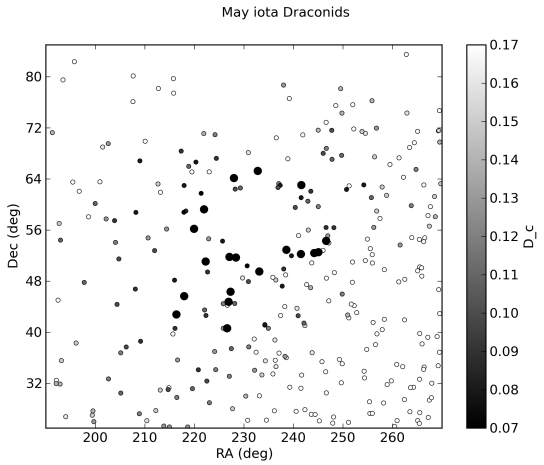

Figure 4 – The radiant plot of the May ι Draconids.

very compact, with average D_{SH} to the mean orbit of only 0.06, and the maximal D_{SH} found is 0.08.

The mean orbit of this shover is similar to the orbit of asteroid 2006 GY2 (see Table 4), indicating possible connection between them.

6 Conclusions

Four possible new meteor showers described in this paper are last ones resulting from our search for new meteor showers. Since all four of them seem to be connected to known parent bodies, a detailed analysis will be done and provided in a separate paper. What is important to point out is that all orbits from which associations had been done are orbits calculated by UFO-Orbit software, which does not take account of meteor deceleration – meaning that average meteor velocity has been used instead of initial velocity. This should not cause any severe errors in the case of swift meteors because the difference between those two values is not large and usually fits well inside observational error margin. However, in case of long lasting slow meteors this may be of importance since true radiant positions may be shifted due to the difference in applied zenith attraction correction, and resulting orbit as well. One may note that the plotted radiants dispersion is really large and no clear radiant drift may be seen - one of reasons for this may be due to not accounting for meteor deceleration, while the other one may lie in the fact that meteoroid streams from these parent bodies suffer from significant perturbations and we see these showers at different positions from year to year. Detailed analysis based on dynamical models, as well as more deceleration accounted orbits should shed more light on this.

Acknowledgements

Our acknowledgments go to all members of Croatian Meteor Network, in alphabetical order (first name first): Alan Pevec, Aleksandar Borojević, Aleksandar Merlak, Alen Žižak, Berislav Bračun, Dalibor Brdarić, Damir Matković, Damir Šegon, Dario Klarić, Dejan Kalebić, Denis Štogl, Denis Vida, Dorian Božićević, Filip Lolić, Filip Novoselnik, Gloryan Grabner, Goran Ljaljić, Ivica Ćiković, Ivica Pletikosa, Janko Mravik, Josip Belas, Korado Korlević, Krunoslav Vardijan, Luka Osokruš, Maja Crnić, Mark Sylvester, Mirjana Malarić, Reiner Stoos, Saša Švagelj, Sonja Janeković, Tomislav Sorić, VSA group 2007, Zvonko Prihoda, Željko Andreić, Željko Arnautović, Željko Krulić.

This work was partially supported by the Faculty of Mining, Geology and Petroleum Engineering, University of Zagreb, Višnjan Science and Education Center and by private funds of CMN members.

References

Drummond J. D. (1981). "A test of comet and meteor shower associations". *Icarus*, **45**, 545–553.

Jopek T. (1993). "Remarks on the meteor orbital similarity D-criterion". *Icarus*, **106**, 603.

Jopek T. J. and Kaňuchová Z. (2014). "Current status of the IAU MDC meteor showers database". In Jopek T. J., Rietmeijer F. J. M., Watanabe J., and Williams I. P., editors, *The Meteoroids 2013, Proceedings of the Astronomical Conference held at A.M. University, Poznań, Poland, Aug. 26-30, 2013*. A.M. University Press, pages 353–364.

Korlević, K Šegon D., Andreić Ž., Novoselnik F., Vida D., and Skokić I. (2013). "Croatian meteor network catalogues of orbits for 2008 and 2009". *WGN, Journal of the IMO*, **41:2**, 48–51.

Šegon D., Gural P., Andreić Ž., Skokić I., Korlević K., Vida D., and Novoselnik F. (2014a). "A parent body search across several video meteor data bases". In Jopek T. J., Rietmeijer F. J. M., Watanabe J., and Williams I. P., editors, *The Meteoroids 2013, Proceedings of the Astronomical Conference held at A.M. University, Poznań, Poland, Aug. 26-30, 2013*. A.M. University Press, pages 251–262.

Šegon D., Gural P., Andreić Ž., Vida D., , Skokić I., Korlević K., and Novoselnik F. (2014b). "Meteor shower search in the CMN and SonotaCo orbital databases". In *Proceedings of the International Meteor Conference, Poznan, Poland, 22-25 August 2013*. International Meteor Organization, pages 97–100.

Šegon D., Andreić Ž., Korlević K., Novoselnik F., and Vida D. (2012). "Croatian Meteor Network Catalogue of Orbits for 2007". *WGN, Journal of the IMO*, **40:3**, 94–97.

SonotaCo (2005-2013). "SonotaCo catalogues 2007-2011". `http://sonotaco.jp/doc/SNM/index.html` .

SonotaCo (2009). "A meteor shower catalog based on video observations in 2007-2008". *WGN, Journal of the IMO*, **37:2**, 55–60.

Southworth R. B. and Hawkins G. S. (1963). "Statistics of meteor streams". *Smithsonian Contr. Astrophys.*, **7**, 261–285.

Šegon D., Gural P., Andreić Ž., Skokić I., Korlević K., Vida D., and Novoselnik F. (2014). "New showers from parent body search across several video meteor databases". *WGN, Journal of the IMO*, **42:2**, 57–64.

Handling Editor: John Correira

Table 5 – Mean orbits of the new showers.

ID	Name	$\lambda_\odot$	$\overline{\lambda_\odot}$	RA	DEC	dRA	dDE	v_g	q	e	ω	Ω	i	N
751 KCE	κ Cepheids	9–21	174.4	318.5	77.5	−1.45	0.39	33.7 ± 1.9	0.983 ± 0.01	0.664 ± 0.041	198.4 ± 5	174.4 ± 4	57.7 ± 3.9	17
753 NED	November Draconids	225–238	232.8	194.2	68.6	1.42	−0.45	42.0 ± 1.2	0.987 ± 0.002	0.701 ± 0.055	183.7 ± 5	232.8 ± 5	73.5 ± 2.3	12
754 POD	ψ Draconids	357–22	11.8	262.3	73.3	2.37	0.25	19.8 ± 1.7	0.994 ± 0.005	0.622 ± 0.035	179.3 ± 10	11.8 ± 7	30.9 ± 3	31
755 MID	May ι Draconids	46–75	60.2	230.8	52.5	0.19	0.62	16.7 ± 2.0	0.989 ± 0.019	0.604 ± 0.043	198.1 ± 9	60.2 ± 7	24.3 ± 4	19

Maribo meteorite and (85182)

David A. J. Seargent[1]

Probable associations are presented between the Maribo meteorite, the Hephaistos-family Apollo asteroid (85182) and the Northern Delta Cancrid meteor shower.

Received 2015 August 18

1 Introduction

On 2009 January 17 at $19^{h}08^{m}28^{s}$ CET, a brilliant fireball was observed travelling in a westerly direction over the Baltic Sea. The event was well observed visually, photographically and by radar, resulting in the subsequent recovery of a small meteorite near the town of Maribo in Denmark. Analysis revealed the broken single stone to be a CM2 chondrite (Haack et al., 2012).

The thorough observational record of the event also permitted the meteoroid's heliocentric orbit to be calculated with a precision which, at that time, was unprecedented for a carbonaceous chondrite. This revealed that the meteoroid had been pursuing an orbit having an unusually small perihelion distance and a remarkable similarity to the Hephaistos family of asteroids. The orbit (J2000) determined for the meteorite (Jenniskens et al., 2012) is; $q = 0.481 \pm 0.010$ AU, $e = 0.795 \pm 0.026$, $\omega = 99\,^{\circ}0 \pm 1\,^{\circ}4$, $\Omega = 117\,^{\circ}64 \pm 0\,^{\circ}05$, $i = 0\,^{\circ}72 \pm 0\,^{\circ}98$.

The D′ criterion (Drummond, 1981) was used to compare this orbit with the Hephaistos asteroids listed by Steel and Asher (1994). The D′ values were larger than the 0.105, considered to be the maximum value for matching orbits, except in the instance of asteroid 1991 AQ (85182) where D′ = 0.04.

As the atmospheric trajectory of the meteorite and the date of its arrival were also consistent with the annual Northern Delta Cancrid meteor shower, its orbit was then compared with the two orbits determined by Z. Sekanina's radar surveys of this shower in 1973 and 1976, and that derived from the photographic survey conducted by B.-A. Lindblad in 1971 and given in Kronk (1988). These three orbits were also compared with that of asteroid 85182. The results are given in Table 1.

2 Conclusion

By comparing the orbits of the Maribo meteorite, asteroid 85182 and the Northern Delta Cancrids using the D′ criterion for orbital association, it was found that;

1. The Hephaistos-family asteroid 85182 is probably the parent body of the Maribo meteorite.
2. The Maribo meteorite was probably a member of the Northern Delta Cancrid meteor shower.
3. Asteroid 85182 is probably the parent body of the Northern Delta Cancrid meteor shower.

References

Drummond J. D. (1981). "A test of comet and meteor shower associations". *Icarus*, **45**, 545–553.

Haack H., Grau T., Bischoff A., Horstmann M., Wasson J., Sorensen A., Laubenstein M., Ott U., Palme H., Gellissen M., Greenwood R. G., Pearson V. E., Franchi I. A., Gabelica Z., and Schmidt-Kopplin P. (2012). "Maribo – a new CM fall from Denmark". *Meteoritics & Planetary Science*, **47**, 30–50.

Jenniskens P., Fries M. D., Yin Q.-Z., Zolensky M., Krot A. N., Sandford S. A., Sears D., Beauford R., Ebel D. S., Friedrich J. M., , Nagashima K., Wimpenny J., Yamakawa A., Nishiizumi K., Hamajima Y., Caffee M. W., Welten K. C., Laubenstein M., Davis A. M., Simon S. B., Heck P. R., Young E. D., Kohl I. E., Thiemens M. H., Nunn M. H., Mikouchi T., Hagiya K., Ohsumi K., Cahill T. A., Lawton J. A., and 40 coauthors (2012). "Radar-enabled recovery of the Sutter's Mill meteorite, a carbonaceous chondrite regolith breccia". *Science*, **338**, 1583–1587.

Kronk G. (1988). *Meteor Showers. A Descriptive Catalog*. Enslow.

Steel D. and Asher D. (1994). "P/Helfenzrieder (1766 II) and the Hephaistos group of Earth-crossing asteroids". *The Observatory*, **114**, 223–226.

Handling Editor: Javor Kac

[1]Email: seargent@ozemail.com.au

IMO bibcode WGN-435-seargent-maribo
NASA-ADS bibcode 2015JIMO...43..151S

Table 1 – Orbits of the Northern Delta Cancrids compared with orbits of Maribo and (85182).

Orbit reference	ω	Ω	i	q	e	D′ (Maribo)	D′(85182)
Sekanina 1973	287.9	292.2	1.2	0.425	0.777	0.066	0.080
Sekanina 1976	291.3	296.4	1.5	0.397	0.783	0.109	0.155
Lindblad 1971	282.6	296.4	0.3	0.448	0.800	0.038	0.060

Preliminary results

Results of the IMO Video Meteor Network — May 2015

Sirko Molau[1], *Javor Kac*[2], *Stefano Crivello*[3], *Enrico Stomeo*[4], *Geert Barentsen*[5], *Rui Goncalves*[6], *Carlos Saraiva*[7], *Maciej Maciejewski*[8], *and Mikhail Maslov*[9]

Observations of the IMO Video Meteor Network are presented for 2015 May. The flux density profile is presented for the η-Aquariids and compared with profiles from 2011–2014. The population index of the 2015 η-Aquariids is calculated for the 6 nights around the shower maximum. The flux density profile is also presented for the η-Lyrids. The 2015 activity profile is consistent with profiles since 2011, and the mean flux density profile covering the years 2011 to 2015 shows the shower peaking at $\lambda = 49\,^{\circ}5$.

Received 2015 August 7

1 Introduction

As in recent years, the weather in May was rather changeable. In particular, during the first few days and for a few days in the second half of May there were larger gaps in the observing statistics. May 3 was particularly poor, with only 171 meteors being recorded in 71 hours of observing time. Only one day so far in 2015 has been less productive – January 29. Despite this, about half of the cameras managed to collect data on twenty or more observing nights during the month. The overall effective observing time dropped to 7 300 hours, during which 16 500 meteors were recorded (Table 1 and Figure 1). The output was lower than in the previous May, but higher than in earlier years.

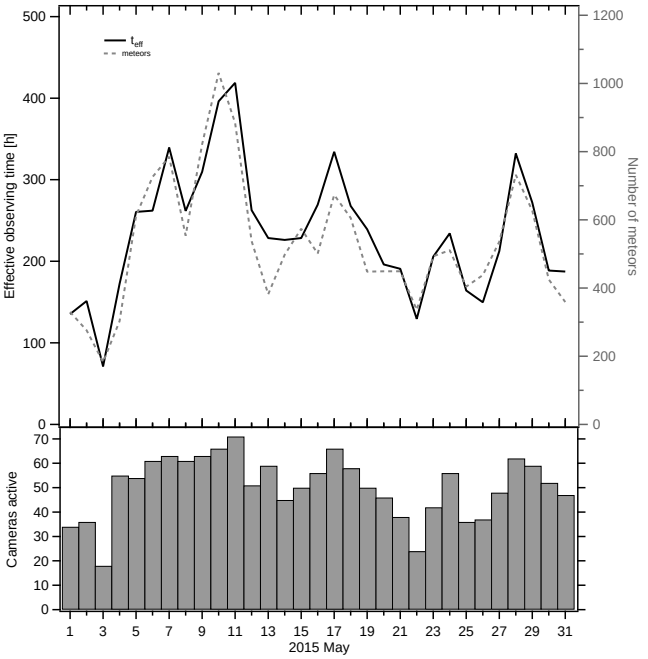

Figure 1 – Monthly summary for the effective observing time (solid black line), number of meteors (dashed gray line) and number of cameras active (bars) in 2015 May.

2 η-Aquariids

Alongside the Orionids, the η-Aquariids of May are the second meteor shower that originates from the well-known comet 1P/Halley. In the last few years we have repeatedly experienced enhanced activity. Figure 2 shows particularly strong outliers in 2012 and 2013 (see Molau et al. (2012) and Molau et al. (2013)). In addition, 2015 also provided a single value that was significantly higher than the surrounding measures. Although not as prominent as in the preceding years, it occurred earlier. At a solar longitude of 43°, the flux density briefly doubles, and then drops back to the long-term average. It is also noticeable that the descending branch starts slightly earlier this year, whereas it was a little late in 2014. The difference between two profiles amounts to 5° in solar longitude.

The population index of the η-Aquariids is about 2.5 at the start and end of the activity period, but in-

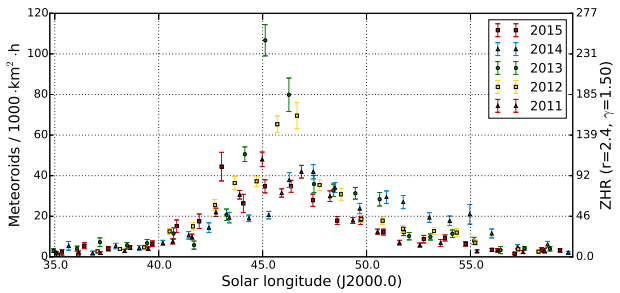

Figure 2 – Flux density profile of the η-Aquariids, obtained from video observations of the IMO Network in May 2011–2015.

[1]Abenstalstr. 13b, 84072 Seysdorf, Germany. Email: sirko@molau.de
[2]Na Ajdov hrib 24, 2310 Slovenska Bistrica, Slovenia. Email: javor.kac@orion-drustvo.si
[3]Via Bobbio 9a/18, 16137 Genova, Italy. Email: stefano.crivello@libero.it
[4]via Umbria 21/d, 30037 Scorze (VE), Italy. Email: stom@iol.it
[5]NASA Ames Research Center, M/S 244-30, Moffett Field, CA 94035, USA. Email: hello@geert.io
[6]Urbanizacao da Boavista, Lote 46, Linhaceira, 2305-114 Asseiceira, Tomar, Portugal. Email: rui.goncalves@ipt.pt
[7]Rua Aquilino Ribeiro, 23 - 1 Dto. 2790028 Carnaxide, Portugal. Email: carlos.saraiva@netcabo.pt
[8]Wolynska 24, 22-100 Chelm, Poland. Email: mazziek@gmail.com
[9]16 Bronny, 90, Novosibirsk, Russia. Email: ast3@ngs.ru

IMO bibcode WGN-435-molau-vidmay
NASA-ADS bibcode 2015JIMO...43..152M

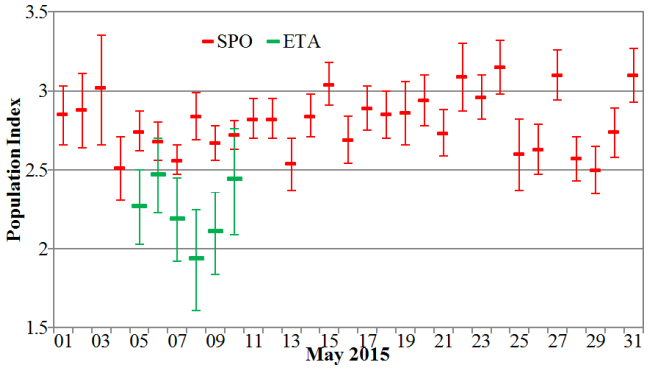

Figure 3 – Population index profile of the η-Aquariids and sporadic meteors in May 2015.

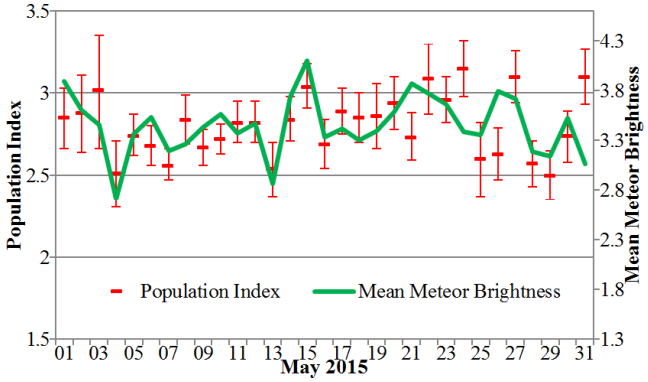

Figure 4 – Population index and mean meteor brightness of sporadic meteors in May 2015.

between it drops to 2.0 (May 8/9). Thus, it is clearly smaller than the population index of sporadic meteors, which, as in previous months, ranges between 2.5 and 3.0 (Figure 3). Towards the end of May there are even values above 3.0, but here the scatter is particularly large.

In addition, the May dataset confirms that the population index profile, which is computed with a complex algorithm (based on the effective collection area and comparison of meteor count of weak and sensitive cameras), correlates well with a very simple measure, namely the average meteor brightness recorded by all cameras. The correlation coefficient between these curves for sporadic meteors in May is 0.5. The challenge is to find the appropriate scales when combining the two graphs. In Figure 4, the mean meteor brightness is plotted on the secondary y-axis and scaled such that mean and variance are identical to the original graph.

3 η-Lyrids

Over the years, the η-Lyrids have shown a rather consistent activity profile, even though they are much weaker than the η-Aquariids (Figure 5).

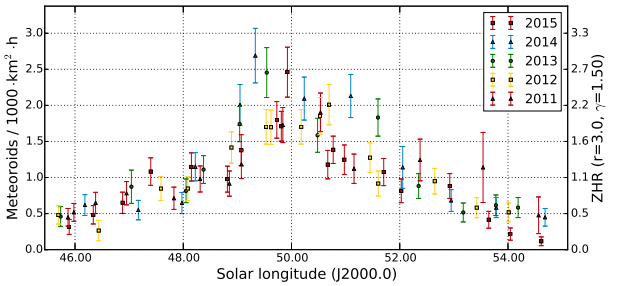

Figure 5 – Flux density profile of the η-Lyrids, obtained from video observations of the IMO Network in May 2011–2015.

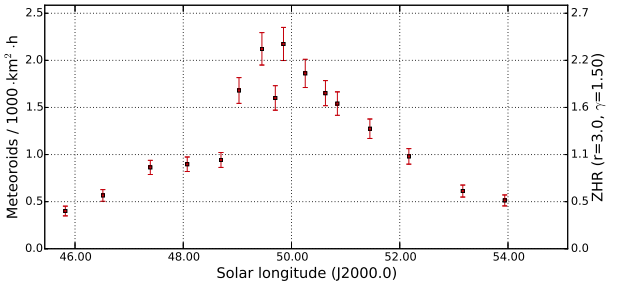

Figure 6 – Mean flux density profile of the η-Lyrids 2011–2015.

The activity interval used by MetRec was too short and, as a result the descending activity branch had to be recomputed. The shower emerges from the sporadic background at about 46° solar longitude , peaks with 2 meteoroids per 1 000 km^2 per hour near $\lambda_\odot = 49\,^\circ\!.5$ and ends at 54° solar longitude. The averaged activity profile (Figure 6) is based on roughly 2 000 shower members.

References

Molau S., Kac J., Berko E., Crivello S., Stomeo E., Igaz A., and Barentsen G. (2012). "Results of the IMO Video Meteor Network – May 2012". *WGN, Journal of the IMO*, **40:4**, 144–148.

Molau S., Kac J., Berko E., Crivello S., Stomeo E., Igaz A., Barentsen G., and Goncalves R. (2013). "Results of the IMO Video Meteor Network – May 2013". *WGN, Journal of the IMO*, **41:4**, 133–138.

Handling Editor: Javor Kac

Code	Name	Location	Camera	FOV [°²]	Stellar LM [mag]	Eff.CA [km²]	Nights	Time [h]	Meteors
ARLRA	Arlt	Ludwigsfelde/DE	Ludwig2 (0.8/8)	1475	6.2	3779	24	127.2	385
BANPE	Bánfalvi	Zalaegerszeg/HU	Huvcse01 (0.95/5)	2423	3.4	361	11	20.4	71
BERER	Berkó	Ludányhalászi/HU	Hulud1 (0.8/3.8)	5542	4.8	3847	12	106.4	293
			Hulud3 (0.95/4)	4357	3.8	876	11	76.6	69
BOMMA	Bombardini	Faenza/IT	Mario (1.2/4.0)	5794	3.3	739	21	147.7	293
BREMA	Breukers	Hengelo/NL	Mbb3 (0.75/6)	2399	4.2	699	17	127.4	119
BRIBE	Klemt	Herne/DE	Hermine (0.8/6)	2374	4.2	678	21	151.6	245
		Bergisch Gladbach/DE	Klemoi (0.8/6)	2286	4.6	1080	23	145.7	227
CASFL	Castellani	Monte Baldo/IT	Bmh1 (0.8/6)	2350	5.0	1611	25	206.2	401
			Bmh2 (1.5/4.5)*	4243	3.0	371	23	188.0	264
CRIST	Crivello	Valbrevenna/IT	Bilbo (0.8/3.8)	5458	4.2	1772	25	169.7	311
			C3P8 (0.8/3.8)	5455	4.2	1586	22	160.6	189
			Stg38 (0.8/3.8)	5614	4.4	2007	26	191.8	614
DONJE	Donani	Faenza/IT	Jenni (1.2/4)	5886	3.9	1222	18	116.1	250
ELTMA	Eltri	Venezia/IT	Met38 (0.8/3.8)	5631	4.3	2151	19	131.7	165
FORKE	Förster	Carlsfeld/DE	Akm3 (0.75/6)	2375	5.1	2154	15	105.8	221
GONRU	Goncalves	Tomar/PT	Templar1 (0.8/6)	2179	5.3	1842	27	207.2	427
			Templar2 (0.8/6)	2080	5.0	1508	27	209.9	365
			Templar3 (0.8/8)	1438	4.3	571	23	175.2	144
			Templar4 (0.8/3.8)	4475	3.0	442	25	189.0	302
			Templar5 (0.75/6)	2312	5.0	2259	26	182.4	281
GOVMI	Govedič	Središče ob Dravi/SI	Orion2 (0.8/8)	1447	5.5	1841	24	162.0	239
			Orion3 (0.95/5)	2665	4.9	2069	15	109.1	100
			Orion4 (0.95/5)	2662	4.3	1043	14	106.6	95
HERCA	Hergenrother	Tucson/US	Salsa3 (0.8/3.8)	2336	4.1	544	29	234.7	392
HINWO	Hinz	Schwarzenberg/DE	Hinwo1 (0.75/6)	2291	5.1	1819	13	102.6	249
IGAAN	Igaz	Debrecen/HU	Hudeb (0.8/3.8)	5522	3.2	620	23	173.4	146
		Hódmezővásárhely/HU	Huhod (0.8/3.8)	5502	3.4	764	22	131.1	113
		Budapest/HU	Hupol (1.2/4)	3790	3.3	475	16	135.2	37
JONKA	Jonas	Budapest/HU	Husor (0.95/4)	2286	3.9	445	23	182.2	146
			Husor2 (0.95/3.5)	2465	3.9	715	19	131.9	97
KACJA	Kac	Ljubljana/SI	Orion1 (0.8/8)	1402	3.8	331	24	155.9	101
		Kamnik/SI	Cvetka (0.8/3.8)*	4914	4.3	1842	16	112.6	256
			Rezika (0.8/6)	2270	4.4	840	19	126.8	424
			Stefka (0.8/3.8)	5471	2.8	379	18	120.2	232
		Kostanjevec/SI	Metka (0.8/12)*	715	6.4	640	1	7.8	7
KISSZ	Kiss	Sülysáp/HU	Husul (0.95/5)*	4295	3.0	355	16	95.3	40
KOSDE	Koschny	Izana Obs./ES	Icc7 (0.85/25)*	714	5.9	1464	12	61.9	339
		La Palma/ES	Icc9 (0.85/25)*	683	6.7	2951	24	151.9	792
		Noordwijkerhout/NL	Lic4 (1.4/50)*	2027	6.0	4509	21	130.5	179
LOJTO	Łojek	Grabniak/PL	Pav57 (1.0/5)	1631	3.5	269	11	73.3	50
LOPAL	Lopes	Lisboa/PT	Naso1 (0.75/6)	2377	3.8	506	10	29.1	56

Table 1 – Observers contributing to 2015 May data of the IMO Video Meteor Network. Eff.CA designates the effective collection area; the overall number of nights is the number of nights with at least one camera operating, the overall observing time and number of meteors are sums over all cameras.

Table 1 – Observers contributing to 2015 May data of the IMO Video Meteor Network – continued from previous page.

Code	Name	Location	Camera	FOV [°²]	Stellar LM [mag]	Eff.CA [km²]	Nights	Time [h]	Meteors
MACMA	Maciejewski	Chełm/PL	Pav35 (0.8/3.8)	5495	4.0	1584	22	149.3	177
			Pav36 (0.8/3.8)*	5668	4.0	1573	24	157.9	280
			Pav43 (0.75/4.5)*	3132	3.1	319	21	158.4	185
			Pav60 (0.75/4.5)	2250	3.1	281	25	153.9	358
MARGR	Maravelias	Lofoupoli-Crete/GR	Loomecon (0.8/12)	738	6.3	2698	13	78.5	60
MARRU	Marques	Lisbon/PT	Cab1 (0.8/3.8)	5291	3.1	467	20	169.6	248
			Ran1 (1.4/4.5)	4405	4.0	1241	24	143.7	242
MASMI	Maslov	Novosibirsk/RU	Nowatec (0.8/3.8)	5574	3.6	773	11	60.5	129
MOLSI	Molau	Seysdorf/DE	Avis2 (1.4/50)*	1230	6.9	6152	22	139.9	686
			Mincam1 (0.8/8)	1477	4.9	1084	22	133.2	315
		Ketzür/DE	Remo1 (0.8/8)	1467	6.5	5491	2	11.6	15
			Remo2 (0.8/8)	1478	6.4	4778	25	139.5	387
			Remo3 (0.8/8)	1420	5.6	1967	18	70.8	158
			Remo4 (0.8/8)	1478	6.5	5358	26	145.2	452
MORJO	Morvai	Fülöpszállás/HU	Huful (1.4/5)	2522	3.5	532	25	180.8	143
MOSFA	Moschner	Rovereto/IT	Rover (1.4/4.5)	3896	4.2	1292	23	34.3	138
OCHPA	Ochner	Albiano/IT	Albiano (1.2/4.5)	2944	3.5	358	13	77.0	99
OTTMI	Otte	Pearl City/US	Orie1 (1.4/5.7)	3837	3.8	460	18	121.1	133
PERZS	Perkó	Becsehely/HU	Hubec (0.8/3.8)*	5498	2.9	460	25	195.2	339
PUCRC	Pucer	Nova vas nad Dragonjo/SI	Mobcam1 (0.75/6)	2398	5.3	2976	18	139.7	139
ROTEC	Rothenberg	Berlin/DE	Armefa (0.8/6)	2366	4.5	911	8	56.0	50
SARAN	Saraiva	Carnaxide/PT	Ro1 (0.75/6)	2362	3.7	381	24	175.0	214
			Ro2 (0.75/6)	2381	3.8	459	26	216.0	302
			Ro3 (0.8/12)	710	5.2	619	28	223.1	425
			Sofia (0.8/12)	738	5.3	907	26	189.9	203
SCHHA	Schremmer	Niederkrüchten/DE	Doraemon (0.8/3.8)	4900	3.0	409	21	128.5	235
SLAST	Slavec	Ljubljana/SI	Kayak1 (1.8/28)	563	6.2	1294	24	165.2	142
			Kayak2 (0.8/12)	741	5.5	920	22	175.2	88
STOEN	Stomeo	Scorze/IT	Min38 (0.8/3.8)	5566	4.8	3270	23	149.4	355
			Noa38 (0.8/3.8)	5609	4.2	1911	24	166.3	366
			Sco38 (0.8/3.8)	5598	4.8	3306	24	170.7	420
STRJO	Strunk	Herford/DE	Mincam2 (0.8/6)	2354	5.4	2751	21	124.7	184
			Mincam3 (0.8/6)	2338	5.5	3590	19	122.8	171
			Mincam4 (1.0/2.6)	9791	2.7	552	22	115.5	108
			Mincam5 (0.8/6)	2349	5.0	1896	19	120.6	158
			Mincam6 (0.8/6)	2395	5.1	2178	22	128.6	138
TEPIS	Tepliczky	Agostyán/HU	Huago (0.75/4.5)	2427	4.4	1036	25	196.9	191
			Humob (0.8/6)	2388	4.8	1607	24	169.9	329
TRIMI	Triglav	Velenje/SI	Sraka (0.8/6)*	2222	4.0	546	21	54.0	131
YRJIL	Yrjölä	Kuusankoski/FI	Finexcam (0.8/6)	2337	5.5	3574	10	73.9	110
ZELZO	Zelko	Budapest/HU	Huvcse03 (1.0/4.5)	2224	4.4	933	12	63.5	65
			Huvcse04 (1.0/4.5)	1484	4.4	573	1	7.6	4
* active field of view smaller than video frame						Overall	31	11 124.1	18 798

Results of the IMO Video Meteor Network — June 2015

Sirko Molau[1], *Javor Kac*[2], *Stefano Crivello*[3], *Enrico Stomeo*[4], *Geert Barentsen*[5], *Rui Goncalves*[6], *Carlos Saraiva*[7], *Maciej Maciejewski*[8], *and Mikhail Maslov*[9]

Observations of the IMO Video Meteor Network are presented for 2015 June. Activity profile is presented for the Daytime Arietids, based on 28 shower meteors. The meteor rate of the Daytime Arietids between June 5 and 11, normalized for the limiting magnitude and angular velocity, is found to be about one quarter of that of the η-Aquariids during their maximum.

Received 2015 September 29

1 Introduction

June presented exceptionally good observing conditions to the meteor observers. There were regional differences, though. In Germany, for example, the observers had to take breaks more frequently, whereas there were perfect observing conditions farther south. 56 of the 80 active cameras managed to observe in twenty or more observing nights, Stg38 and Jenni in Italy even observed without any break. The last night of June was the most successful one with over 70 active video cameras.

The effective observing time in June accumulated to exactly 7 000 hours, slightly more than in the previous year. With 18 500, however, the total number of meteors was slightly lower than in 2014 (Table 1 and Figure 1). According to the long-term statistics, June could close the gap to the other months in the first half year. For every month we meanwhile store over 100 000 single-station meteors in the IMO Video Meteor Database – only February still falls short by a mere 3 000 meteors.

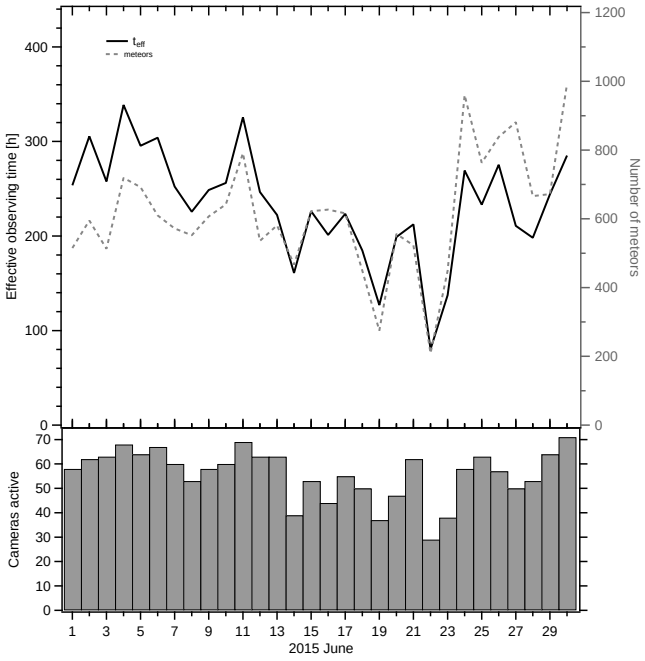

Figure 1 – Monthly summary for the effective observing time (solid black line), number of meteors (dashed gray line) and number of cameras active (bars) in 2015 June.

2 Daytime Arietids

The "Daytime Arietids campaign" initiated by Jürgen Rendtel (2014) remains a real challenge. It is well known that this is one of the strongest radio meteor showers, but can it also compete with the major showers of visual observers like the Quadrantids, Perseids and Geminids? That shall be investigated with the help of optical observations. The observation of this shower is quite demanding, since the radiant lies just 30° away from the Sun and reaches sufficient altitude only at broad twilight. The analysis of observations, however, is similarly complicated. Due to the low radiant altitude and limiting magnitude, there are automatically large correction factors. Minor systematic errors are significantly blown up under such circumstances.

Between 2015 June 5 and 11, we recorded 28 Daytime Arietids. They were quite evenly distributed over the solar longitude, and also the average profile made of roughly 100 meteors from the last five years is relatively flat (Figure 2). The flux density is of the order of 10

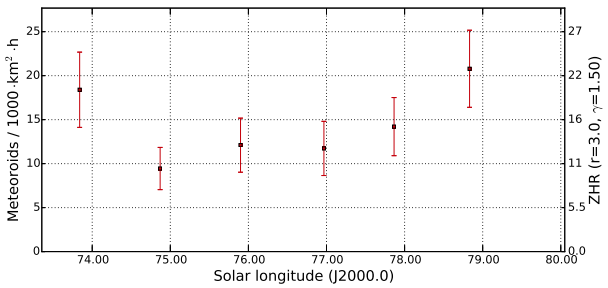

Figure 2 – Averaged flux density profile of the Daytime Arietids in the years 2011 to 2015.

[1]Abenstalstr. 13b, 84072 Seysdorf, Germany. Email: sirko@molau.de
[2]Na Ajdov hrib 24, 2310 Slovenska Bistrica, Slovenia. Email: javor.kac@orion-drustvo.si
[3]Via Bobbio 9a/18, 16137 Genova, Italy. Email: stefano.crivello@libero.it
[4]via Umbria 21/d, 30037 Scorze (VE), Italy. Email: stom@iol.it
[5]NASA Ames Research Center, M/S 244-30, Moffett Field, CA 94035, USA. Email: hello@geert.io
[6]Urbanizacao da Boavista, Lote 46, Linhaceira, 2305-114 Asseiceira, Tomar, Portugal. Email: rui.goncalves@ipt.pt
[7]Rua Aquilino Ribeiro, 23 - 1 Dto. 2790028 Carnaxide, Portugal. Email: carlos.saraiva@netcabo.pt
[8]Wolynska 24, 22-100 Chelm, Poland. Email: mazziek@gmail.com
[9]16 Bronny, 90, Novosibirsk, Russia. Email: ast3@ngs.ru

IMO bibcode WGN-435-molau-vidjun
NASA-ADS bibcode 2015JIMO...43..156M

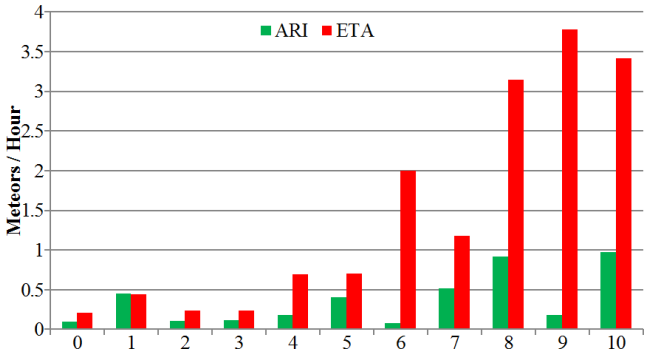

Figure 3 – Average number of Daytime Arietids and η-Aquariids per hour at a given radiant altitude, normalized for the same limiting magnitude and angular meteor velocity.

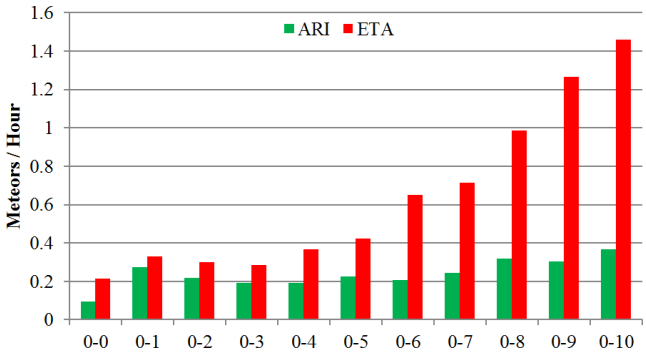

Figure 4 – Same as Figure 3, but with cumulative increasing radiant altitude.

meteoroids per 1 000 km^2 per hour. Given a population index of $r = 3.0$ and a zenith exponent of $\gamma = 1.0$, a ZHR of the order of 5 is obtained. At a population index $r = 2.0$ and zenith exponent of $\gamma = 2.0$, however, the ZHR jumps to a staggering 250. So the fluctuation margin is by a factor of 50. That underlines perfectly that the real challenge is not to observe these meteors but rather to obtain reliable information about the Daytime Arietid activity under such extreme circumstances.

To get an impression about the real activity of the Daytime Arietids we compared it with the η-Aquariids. The radiant of the latter shower also reaches a significant altitude only at dawn in the mid-northern latitudes, but thanks to better observing conditions in the south we have a more reliable picture of its zenithal hourly rate.

We analysed the time of peak activity of the η-Aquariids (May 3–8) and the above-mentioned activity interval of the Daytime Arietids (2015 June 5–11). We omitted intervals with limiting stellar magnitude of zero. For both showers we obtained a histogram showing the number of meteors recorded per degree radiant altitude. In parallel we calculated the observing time and average limiting magnitude of all cameras per radiant altitude interval.

Comparing the mean number of observed shower meteors per hour we get a first hint on the real activity of the Daytime Arietids. However, two additional effects have to be taken into consideration:

- In case of the Daytime Arietids, twilight has progressed further, which is reflected by decreasing limiting magnitudes. Indeed, the average stellar limiting magnitude reduces from an average 4.1 mag (0° radiant altitude) to 3.3 mag (10° radiant altitude), whereas it remains constant at 3.7 mag in case of the η-Aquariids.

- The Daytime Arietids are slower than the η-Aquariids. The loss in the limiting magnitude for the meteors caused by the meteor motion amount to 1.3 mag for the Daytime Arietids, but 1.5 mag for the η-Aquariids.

If these effects are accounted for with a population index of 3.0 (whereby the effect of the r-value is not so high this time, because the difference in limiting magnitude between both showers does not exceed 0.5 mag), we obtain Figure 3. It becomes clear that at a similar radiant altitude we recorded more η-Aquariids per hour than Daytime Arietids.

Due to the low meteor counts, there is significant scatter in the normalized meteor rates. For this reason we depicted cumulative averages in Figure 4, i.e. not the average activity at a fixed radiant altitude h but in the interval 0° to h°. From this we can conclude that the activity of the Daytime Arietids is only about a quarter of the η-Aquariid activity. That is not a precise measure of flux density or ZHR, but at least an estimate that is independent of the radiant altitude. We can conclude that the Daytime Arietids are less spectacular in the optical than in the radar domain. Their population index must be higher than those of the well-known major showers in the optical domain.

3 The Daytime Arietid that was not

Finally we want to give an illustrative example, that meteor shower assignment in the case of single-station video or visual observation can be erroneous, since it lacks spatial information from the meteor trail. That is not a remarkably new finding, but sometimes still educational.

When analyzing the Daytime Arietids, Sirko Molau recognized that his camera Remo2 in Ketzür/Germany had recorded one of these rare shower members on June 8 at $00^h57^m42^s$ UT (Figure 5, left). The train ended left of Atair (α Aquilae) and the backward prolongation missed the radiant by only 0.°3. That is a supposedly safe shower assignment, even though the apparent velocity was 19°/s, about 4°/s higher than expected.

Fortunately it was not just Remo2 that recorded that meteor, because the camera Ludwig2 of Rainer Arlt covered the same atmospheric volume at the observing site in Ludwigsfelde, which is about 50 km away. Indeed also this camera had recorded a similar meteor at exactly the same second (Figure 5, right), which crossed the right wing of the eagle. It all seems to argue that both cameras recorded the same meteor, but Ludwig2 flagged its meteor as sporadic.

An evil thought is immediately thrilling through the programmer: Is there a bug in the software? So you start to frantically check the observation and verify the

Figure 5 – Bright meteor in the morning of 2015 June 8, recorded by Remo2 (left) in Ketzür, Germany and by Ludwig2 (right) at about 50 km distance in Ludwigsfelde, Germany.

code. The average meteor trail is correctly determined as can be shown by a manual verification. So it must be the velocity determination, which shows indeed some discrepancies that cannot be sorted out on short notice. The analysis is postponed until the next evening, but overnight you realize what a catastrophic impact that would have on all analyses provided so far. Fortunately there is an all clear signal at the next evening, because the error was made during the verification. The value obtained by MetRec fits perfectly.

Then you realize that the radiant distance of the Remo2 meteor is slightly below 90° and of the Ludwig2 meteor slightly above 90°. Is there a problem with meteor shower assignment beyond 90° radiant distance? Again your thoughts pivot around which severe implication this would have until the all clear signal lights up once more. If the accepted errors in meteor shower assignment are increased, also the meteor of Ludwig2 is recognized as Daytime Arietid. The radiant miss distance is almost 8° and with 24°/s the angular velocity is even 6°/s higher than expected. Final clarification comes from a quick and dirty hack that computes the intersection point of the backward prolongation of two meteors. The radiant position is obtained as $\alpha = 0^{\mathrm{h}}43$ and $\delta = 27°$. The velocity has to be increased to $V_\infty = 70$ km/s. Voilà! Now both meteors are matching perfectly to the radiant.

So the true radiant is about 30° away from the radiant of the Daytime Arietids! It was pure chance that the backward prolongation of Remo2 meteor matched exactly to the radiant of ARI. Only the recording of a second camera revealed the true origin of the meteor.

In the end the programmer is left with the warm feeling, that about 15 years earlier he had sufficiently tested and created quite reliable source code (at least in this respect).

References

Rendtel J. (2014). "Daytime meteor showers". In Rault J.-L. and Roggemans P., editors, *Proceedings of the International Meteor Conference, Giron, France, 18-21 September 2014*. pages 93–97.

Handling Editor: Javor Kac

Code	Name	Location	Camera	FOV [°²]	Stellar LM [mag]	Eff.CA [km²]	Nights	Time [h]	Meteors
ARLRA	Arlt	Ludwigsfelde/DE	Ludwig2 (0.8/8)	1475	6.2	3779	20	59.1	286
BANPE	Bánfalvi	Zalaegerszeg/HU	Huvcse01 (0.95/5)	2423	3.4	361	16	13.1	87
BERER	Berkó	Ludányhalászi/HU	Hulud1 (0.8/3.8)	5542	4.8	3847	6	25.8	112
			Hulud3 (0.95/4)	4357	3.8	876	5	24.6	38
BOMMA	Bombardini	Faenza/IT	Mario (1.2/4.0)	5794	3.3	739	29	126.4	401
BREMA	Breukers	Hengelo/NL	Mbb3 (0.75/6)	2399	4.2	699	17	61.9	157
BRIBE	Klemt	Herne/DE	Hermine (0.8/6)	2374	4.2	678	18	64.9	186
		Bergisch Gladbach/DE	Klemoi (0.8/6)	2286	4.6	1080	22	67.3	146
CASFL	Castellani	Monte Baldo/IT	Bmh1 (0.8/6)	2350	5.0	1611	25	117.6	248
			Bmh2 (1.5/4.5)*	4243	3.0	371	25	92.5	147
CRIST	Crivello	Valbrevenna/IT	Bilbo (0.8/3.8)	5458	4.2	1772	28	137.4	294
			C3P8 (0.8/3.8)	5455	4.2	1586	24	113.7	234
			Stg38 (0.8/3.8)	5614	4.4	2007	30	151.1	629
DONJE	Donani	Faenza/IT	Jenni (1.2/4)	5886	3.9	1222	30	167.1	637
ELTMA	Eltri	Venezia/IT	Met38 (0.8/3.8)	5631	4.3	2151	23	85.0	214
FORKE	Förster	Carlsfeld/DE	Akm3 (0.75/6)	2375	5.1	2154	18	57.4	161
GONRU	Goncalves	Tomar/PT	Templar1 (0.8/6)	2179	5.3	1842	26	168.8	535
			Templar2 (0.8/6)	2080	5.0	1508	26	171.3	382
			Templar3 (0.8/8)	1438	4.3	571	25	150.3	149
			Templar4 (0.8/3.8)	4475	3.0	442	27	164.9	374
			Templar5 (0.75/6)	2312	5.0	2259	24	149.8	333
GOVMI	Govedič	Središče ob Dravi/SI	Orion2 (0.8/8)	1447	5.5	1841	18	74.2	209
HERCA	Hergenrother	Tucson/US	Salsa3 (0.8/3.8)	2336	4.1	544	27	175.3	320
HINWO	Hinz	Schwarzenberg/DE	Hinwo1 (0.75/6)	2291	5.1	1819	19	67.6	178
IGAAN	Igaz	Debrecen/HU	Hudeb (0.8/3.8)	5522	3.2	620	23	104.4	112
		Hódmezővásárhely/HU	Huhod (0.8/3.8)	5502	3.4	764	19	67.1	89
		Budapest/HU	Hupol (1.2/4)	3790	3.3	475	18	37.7	49
JONKA	Jonas	Budapest/HU	Husor (0.95/4)	2286	3.9	445	21	80.4	109
			Husor2 (0.95/3.5)	2465	3.9	715	21	96.8	103
KACJA	Kac	Ljubljana/SI	Orion1 (0.8/8)	1402	3.8	331	20	82.3	95
		Kamnik/SI	Cvetka (0.8/3.8)*	4914	4.3	1842	22	88.2	317
			Rezika (0.8/6)	2270	4.4	840	22	89.9	381
			Stefka (0.8/3.8)	5471	2.8	379	21	80.7	188
		Kostanjevec/SI	Metka (0.8/12)*	715	6.4	640	3	16.2	22
KISSZ	Kiss	Sülysáp/HU	Husul (0.95/5)*	4295	3.0	355	22	90.0	68
KOSDE	Koschny	Izana Obs./ES	Icc7 (0.85/25)*	714	5.9	1464	24	119.8	664
		La Palma/ES	Icc9 (0.85/25)*	683	6.7	2951	27	152.9	1145
		Noordwijkerhout/NL	Lic4 (1.4/50)*	2027	6.0	4509	22	14.8	87
LOJTO	Łojek	Grabniak/PL	Pav57 (1.0/5)	1631	3.5	269	9	31.5	30

Table 1 – Observers contributing to 2015 June data of the IMO Video Meteor Network. Eff.CA designates the effective collection area; the overall number of nights is the number of nights with at least one camera operating, the overall observing time and number of meteors are sums over all cameras.

Table 1 – Observers contributing to 2015 June data of the IMO Video Meteor Network – continued from previous page.

Code	Name	Location	Camera	FOV [°²]	Stellar LM [mag]	Eff.CA [km²]	Nights	Time [h]	Meteors
MACMA	Maciejewski	Chełm/PL	Pav35 (0.8/3.8)	5495	4.0	1584	24	85.6	367
			Pav36 (0.8/3.8)*	5668	4.0	1573	24	89.4	259
			Pav43 (0.75/4.5)*	3132	3.1	319	22	85.8	181
			Pav60 (0.75/4.5)	2250	3.1	281	25	94.6	329
MARGR	Maravelias	Lofoupoli-Crete/GR	Loomecon (0.8/12)	738	6.3	2698	22	150.7	325
MARRU	Marques	Lisbon/PT	Cab1 (0.8/3.8)	5291	3.1	467	23	146.8	262
			Ran1 (1.4/4.5)	4405	4.0	1241	25	148.2	235
MASMI	Maslov	Novosibirsk/RU	Nowatec (0.8/3.8)	5574	3.6	773	21	25.9	80
MOLSI	Molau	Seysdorf/DE	Avis2 (1.4/50)*	1230	6.9	6152	20	69.3	351
			Escimo2 (0.85/25)	155	8.1	3415	19	59.4	142
			Mincam1 (0.8/8)	1477	4.9	1084	17	53.8	210
		Ketzür/DE	Remo1 (0.8/8)	1467	6.5	5491	19	67.1	331
			Remo2 (0.8/8)	1478	6.4	4778	19	64.7	262
			Remo3 (0.8/8)	1420	5.6	1967	17	55.0	117
			Remo4 (0.8/8)	1478	6.5	5358	17	64.7	340
MOSFA	Moschner	Rovereto/IT	Rover (1.4/4.5)	3896	4.2	1292	24	19.8	130
OCHPA	Ochner	Albiano/IT	Albiano (1.2/4.5)	2944	3.5	358	20	57.4	98
OTTMI	Otte	Pearl City/US	Orie1 (1.4/5.7)	3837	3.8	460	22	90.0	131
PERZS	Perkó	Becsehely/HU	Hubec (0.8/3.8)*	5498	2.9	460	27	128.1	336
PUCRC	Pucer	Nova vas nad Dragonjo/SI	Mobcam1 (0.75/6)	2398	5.3	2976	21	90.1	168
ROTEC	Rothenberg	Berlin/DE	Armefa (0.8/6)	2366	4.5	911	8	26.9	62
SARAN	Saraiva	Carnaxide/PT	Ro1 (0.75/6)	2362	3.7	381	21	121.7	214
			Ro2 (0.75/6)	2381	3.8	459	24	146.9	302
			Ro3 (0.8/12)	710	5.2	619	22	131.2	344
			Sofia (0.8/12)	738	5.3	907	24	99.0	166
SCALE	Scarpa	Alberoni/IT	Leo (1.2/4.5)*	4152	4.5	2052	19	67.3	103
SCHHA	Schremmer	Niederkrüchten/DE	Doraemon (0.8/3.8)	4900	3.0	409	21	65.5	159
SLAST	Slavec	Ljubljana/SI	Kayak1 (1.8/28)	563	6.2	1294	25	111.9	222
			Kayak2 (0.8/12)	741	5.5	920	22	110.4	89
STOEN	Stomeo	Scorze/IT	Min38 (0.8/3.8)	5566	4.8	3270	23	73.8	325
			Noa38 (0.8/3.8)	5609	4.2	1911	27	100.3	311
			Sco38 (0.8/3.8)	5598	4.8	3306	27	97.6	366
STRJO	Strunk	Herford/DE	Mincam2 (0.8/6)	2354	5.4	2751	16	65.0	180
			Mincam3 (0.8/6)	2338	5.5	3590	20	63.3	158
			Mincam4 (1.0/2.6)	9791	2.7	552	20	62.2	104
			Mincam5 (0.8/6)	2349	5.0	1896	16	62.6	139
			Mincam6 (0.8/6)	2395	5.1	2178	18	63.5	126
TEPIS	Tepliczky	Agostyán/HU	Huago (0.75/4.5)	2427	4.4	1036	25	114.9	122
			Humob (0.8/6)	2388	4.8	1607	25	75.4	276
TRIMI	Triglav	Velenje/SI	Sraka (0.8/6)*	2222	4.0	546	23	50.5	143
ZELZO	Zelko	Budapest/HU	Huvcse03 (1.0/4.5)	2224	4.4	933	2	4.3	9
						Overall	30	7 000.4	18 490

* active field of view smaller than video frame

The International Meteor Organization

web site http://www.imo.net

Council

President: Cis Verbeeck,
Bogaertsheide 5, 2560 Kessel, Belgium.
e-mail: cis.verbeeck@scarlet.be

Vice-President: Jürgen Rendtel,
Eschenweg 16, D-14476 Marquardt, Germany.
tel. +49 33208 50753
e-mail: jrendtel@aip.de

Secretary-General: Robert Lunsford,
1828 Cobblecreek Street, Chula Vista,
CA 91913-3917, USA. tel. +1 619 585 9642
e-mail: lunro.imo.usa@cox.net

Treasurer: Marc Gyssens, Heerbaan 74,
B-2530 Boechout, Belgium.
e-mail: marc.gyssens@uhasselt.be
BIC: GEBABEBB
IBAN: BE30 0014 7327 5911
Always state BIC and IBAN codes together!
Check international transfer charges with your bank; you are responsible for paying these.

Other Council members:

David Asher, Armagh Observatory, College Hill, Armagh, Northern Ireland BT61 9DG, UK.
e-mail: dja@arm.ac.uk

Geert Barentsen, NASA Ames Research Center, M/S 244-30, Moffett Field CA 94035, USA.
e-mail: hello@geert.io

Javor Kac (see details under WGN)

Detlef Koschny, Zeestraat 46,
NL-2211 XH Noordwijkerhout, Netherlands.
e-mail: detlef.koschny@esa.int

Sirko Molau, Abenstalstraße 13b, D-84072 Seysdorf, Germany. e-mail: sirko@molau.de

Jean-Louis Rault, Société Astronomique de France, 16, rue de la Vallée, 91360 Epinay sur Orge, France. e-mail: f6agr@orange.fr

Paul Roggemans (see details under IMC Liaison Officer)

Commission Directors

Visual Commission: Rainer Arlt (rarlt@aip.de)
Generic e-mail address: visual@imo.net
Electronic visual report form:
http://www.imo.net/visual/report/electronic

Video Commission: Sirko Molau (sirko@molau.de)
Generic e-mail address: video@imo.net

Photographic Commission: Bill Ward (William.Ward@glasgow.ac.uk)
Generic e-mail address: photo@imo.net

Radio Commission: Jean-Louis Rault (f6agr@orange.fr)
Generic e-mail address: radio@imo.net

Fireballs: Online fireball reports:
http://fireballs.imo.net

IMC Liaison Officer

Paul Roggemans, Pijnboomstraat 25, 2800 Mechelen, Belgium, e-mail: paul.roggemans@gmail.com

WGN

Editor-in-chief: Javor Kac
Na Ajdov hrib 24, SI-2310 Slovenska Bistrica, Slovenia. e-mail: wgn@imo.net;
include METEOR in the e-mail subject line

Editorial board: Ž. Andreić, M. Argo, D.J. Asher, J. Correira, M. Gyssens, H.V. Hendrix, C. Hergenrother, T. Markham, J. Rendtel, J.-L. Rault, P. Roggemans, C. Verbeeck.

IMO Sales

Available from the Treasurer or the Electronic Shop on the IMO Website	€	$
IMO membership, including subscription to WGN Vol. 43 (2015)		
Surface mail	26	39
Air Mail (outside Europe only)	49	69
Electronic subscription only	21	29
Back issues of WGN on paper (price per complete volume)		
Vols. 26 (1998) – 35 (2007) except 30 (2002), 38 (2010) – 42 (2014)	15	23
Vols. 37 (2009) – 42 (2014) – electronic version only	9	13
Proceedings of the International Meteor Conference on paper		
1990, 1991, 1993, 1995, 1996, 1999, 2000, 2002, 2003, per year	9	13
2007, 2010, 2011, per year	15	23
2012, 2013, 2014, 2015 per year	25	37
Proceedings of the Meteor Orbit Determination Workshop 2006	15	23
Radio Meteor School Proceedings 2005	15	23
Handbook for Meteor Observers	15	23
Meteor Shower Workbook	12	18
Electronic media		
Meteor Beliefs Project CD-ROM	6	9
DVD: WGN Vols. 6–30 & IMC 1991, 1993–96, 2001–04	45	69

Orionid fireball on 2015 October 23 over Slovenia

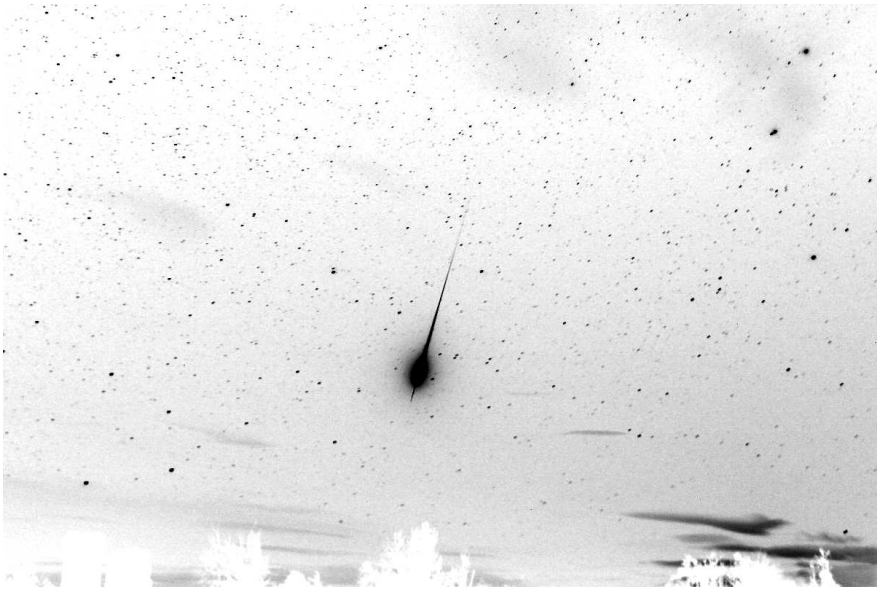

02:44 UT

02:45 UT

02:46 UT

02:47 UT

02:48 UT

02:49 UT

02:50 UT

02:51 UT

02:52 UT

This Orionid fireball on 2015 October 23 at $02^{\mathrm{h}}42^{\mathrm{m}}45^{\mathrm{s}}$ UT appeared low in the north as viewed from Medvedje Brdo, Slovenia. The persistent train could be followed for 4 minutes with the naked eye and for 50 minutes on photographs, until clouds covered it. The photographs were shot using Canon 40D camera set at ISO 800 equipped with 17 mm $f/2.8$ lens, and exposures of 59 s. Photos courtesy of Javor Kac.